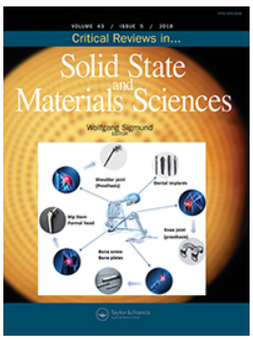

Taylor & Francis
Taylor & Francis Group

Critical Reviews in Solid State and Materials Sciences

ISSN: 1040-8436 (Print) 1547-6561 (Online) Journal homepage: http://www.tandfonline.com/loi/bsms20

Phase-Field Modelling in Extractive Metallurgy

Inge Bellemans, Nele Moelans & Kim Verbeken

To cite this article: Inge Bellemans, Nele Moelans & Kim Verbeken (2018) Phase-Field Modelling in Extractive Metallurgy, Critical Reviews in Solid State and Materials Sciences, 43:5, 417-454, DOI: 10.1080/10408436.2017.1397500

To link to this article: https://doi.org/10.1080/10408436.2017.1397500

Published online: 04 Dec 2017.

CRITICAL REVIEWS IN SOLID STATE AND MATERIALS SCIENCES
2018, VOL. 43, NO. 5, 417–454
https://doi.org/10.1080/10408436.2017.1397500

Taylor & Francis
Taylor & Francis Group

Phase-Field Modelling in Extractive Metallurgy

Inge Bellemans [a], Nele Moelans[b], and Kim Verbeken[a]

[a]Department of Materials, Textiles and Chemical Engineering, Ghent University, Ghent, Belgium; [b]Department of Materials Engineering, KU Leuven, Leuven, Belgium

ABSTRACT

The phase-field method has already proven its usefulness to simulate microstructural evolution for several applications, e.g., during solidification, solid-state phase transformations, fracture, etc. This wide variety of applications follows from its diffuse-interface approach. Moreover, it is straightforward to take different driving forces into account. The purpose of this paper is to give an introduction to the phase-field modelling technique with particular attention for models describing phenomena important in extractive metallurgy. The concept of diffuse interfaces, the phase-field variables, the thermodynamic driving force for microstructure evolution and the phase-field equations are discussed. Some of the possibilities to solve the equations describing microstructural evolution are also described, followed by possibilities to make the phase-field models quantitative and the phase-field modelling of the microstructural phenomena important in extractive metallurgy, i.e., multiphase field models. Finally, this paper illustrates how the phase-field method can be applied to simulate several processes taking place in extractive metallurgy and how the models can contribute to the further development or improvement of these processes.

KEYWORDS

Phase field model; microstructure evolution; extractive metallurgy

Table of Contents

CONTACT Inge Bellemans inge.bellemans@ugent.be

Color versions of one or more of the figures in the article can be found online at www.tandfonline.com/bsms.

1. The general technique of phase-field modelling

The phase-field method already proved to be a very powerful, flexible and versatile modelling technique for microstructural evolution (e.g., solidification,[1–3] solid-state phase transformations,[4] solid-state sintering,[5] grain growth,[6] dislocation dynamics,[7] crack propagation,[8,9] electromigration,[10] etc.). The phase-field method is also eye-catching because it produces remarkable visual outputs, particularly of morphology, capturing features which are often realistic in appearance.[11,12]

Phase-field models are phenomenological continuum field approaches with the ability to model and predict mesoscale morphological and microstructure evolution in materials at the nanoscopic and mesoscopic level.[4,11,13] In contrast to macroscopic models, the crystallization kinetics, diffusion profiles, and the morphology of individual crystals can be described.[3]

Macroscopic models usually rely on thermodynamic equilibrium calculations, but phase-field models are based upon the principles of irreversible thermodynamics to describe evolving microstructures.[3] Phase-field models can be regarded as a set of kinetic equations and because they do not only predict the final thermodynamic equilibrium states but also realistic microstructures, these models should consider several contributions to the thermodynamic functions and kinetics involved. The thermodynamics of phase transformation phenomena determine the general direction of microstructure evolution, ultimately eliminating all nonequilibrium defects, but the kinetics determine the actual microstructural path. This can lead the system through a series of nonequilibrium microstructural states.[11] The total free energy of a system, which is minimized toward equilibrium, is defined as the integral of the local energy density, which traditionally includes interfacial energies and chemical energies of the bulk phases, but also elastic or magnetic energy contributions can be included. The method can in principle deal with a large number of interacting phenomena, because of the inclusion of various energy contributions.[12–14] Phase-field models describe a microstructure, both the compositional/structural domains and the interfaces, as a whole by using a set of field variables.[4] These field variables are continuous spatial functions changing smoothly and not sharply across internal interfaces, i.e., diffuse interfaces.[4,11,13,14]

A characteristic feature of the phase-field method is that its equation can often be written down following simple rules or intuition, but that detailed properties (which have to be known if quantitative simulations are desired) become apparent only through a mathematical analysis that can be quite intricate. Therefore, it is not always easy to perceive the limits of applicability of the phase-field method.[15] Several problems remain[12]: interface width is an adjustable parameter which may be set to physically unrealistic values to bridge the scale gap between the thickness of the physical interfaces and the typical scale of the microstructures, which may result in loss of detail and unphysical interactions between different interfaces. Therefore, to guarantee precise simulations, all these effects have to be controlled and, if possible, eliminated. This is done in the so-called thin-interface limit (cf. infra): the equations of the phase-field model are analyzed under the assumption that the interface thickness is much smaller than any other physical length-scale present in the problem, but otherwise arbitrary. The procedure of matched asymptotic expansions then yields the effective boundary conditions valid at the macroscale, which contain all effects of the finite interface thickness up to the order to which the expansions are carried out.[15] Moreover, it is not clear at what point the assumptions of irreversible thermodynamics, on which the equations describing microstructural evolution are based, would fail. The free energy expression originates from a Taylor expansion,[16] of which it is not clear to which extent it remains valid. The definition of the free energy density variation in the boundary is sometimes claimed to be somewhat arbitrary and assumes the existence of systematic gradients within the interface. Some say, however, that there is no physical justification

for this assumed form in many cases. However, in a liquid–gas system, for example, the density varies continuously over the interface and thus a diffuse interface between stable phases of a material can be seen as more natural than the assumption of a sharp interface with a discontinuity in at least one property of the material.

The text first discusses the concept of diffuse interfaces, the phase-field variables, the thermodynamic driving force for microstructural evolution and the phase-field equations. Some of the possibilities to solve the equations describing microstructural evolution are also described, followed by possibilities to make the phase-field models quantitative.

In extractive metallurgy, the processes are subdivided into 3 categories: pyrometallurgy, hydrometallurgy and electrometallurgy. Pyrometallurgy involves high temperature processes, hydrometallurgy involves aqueous solutions and electrometallurgy involves electrochemistry to extract the metals. In pyrometallurgy, typically several phases are present and it is the distribution of the various elements between these phases that determines the extractive nature of the process under consideration. Thus, the developments of multiphase field models are especially relevant. Moreover, as some phases are liquid and others solid, the process of solidification also plays an important role in pyrometallurgy. Therefore, this paper gives a historical overview toward the development of multiphase-field models and models for solidification, as this illustrates the importance of the different developments, e.g., the thin-interface limit, the quasi-equilibrium condition and the anti-trapping current. In hydrometallurgy, mostly the partitioning or the distribution of the elements over the different phases is important and phase-field modelling has not yet been applied, to the author's knowledge, to this type of processes. This is in contrast with electrometallurgy, which considers, on the one hand, the double layer level and the mesoscopic level, on the other hand, in several phase-field models. Again, for the latter cases, the thin-interface limit is important and finite interface dissipation will become as well. Finally, this paper illustrates how the phase-field method can be applied to simulate several processes taking place in extractive metallurgy and how the models can contribute to the further development or improvement of these processes.

1.1. Variables

The microstructures considered in phase-field simulations typically consist of a number of grains or phases. The shape and distribution of these grains is represented by functions that are continuous in space and time and are called phase-field variables.[14,17] The dependence of the variables on the spatial coordinates enables prescribing composition and phase-fields that are heterogeneous within the system and allows simulating both the kinetics and the resulting morphology associated with phase transformations.[11] Characteristic about the phase-field method is its diffuse-interface approach. At interfaces, the field variables vary smoothly over a transition/spatial gradient of the phase-field variables between the equilibrium values in the neighboring grains or phases in a narrow region (the right side of Figure 1).[4,11]

In classical sharp interface models for microstructure evolution, on the other hand, the model equations are defined in a homogeneous part of the microstructure, e.g., a single grain of a certain phase. At the interfaces (with zero-width, as shown on the left of Figure 1), the properties change discontinuously from one bulk value to another and certain constraints are applied locally at the interfaces such as local thermodynamic equilibrium and heat or mass balances. The interfaces move as the microstructure evolves, which gives this type of free-boundary problems their name: moving-boundary problems, sometimes also referred to as the Stefan problem.[13,18] Therefore, the interfaces need to be explicitly tracked, which does not facilitate the model formulation and numerical implementation. This is why sharp-interface simulations are mostly restricted to one-dimensional systems or simplified morphologies.[4,12–14]

In a phase-field model (on the right in Figure 1), explicit tracking of individual interfaces or phase boundaries is avoided by assuming diffuse interfaces, where the state variables vary in a steep but continuous way over a narrow interface region.[12] This 'smear out' of the variable can for example be interpreted as a physical decrease of structure in a solid–liquid interface on an atomic scale.[19] The position of the interfaces is implicitly given by the value of the phase-field variables.[12] In this way the mathematically difficult problems of applying boundary conditions at an interface whose position is part of the unknown solution, is avoided. Thus, the evolution of complex morphologies can be predicted without making any assumption on the shape of the grains. Moreover, in

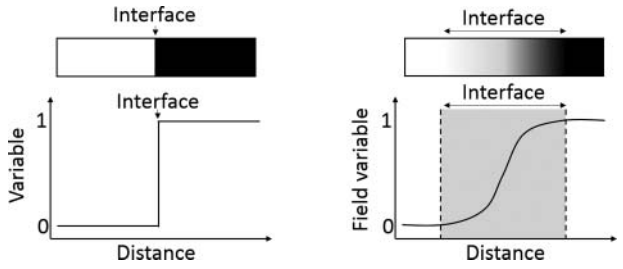

Figure 1. Schematic one-dimensional representation of a sharp (left) and of a diffuse (right) interface.[12,14]

a diffuse interface model, the model equations, for example for solute diffusion, are defined over the whole system, thus the number of equations to be solved is far smaller.[3]

The field variables do not correspond to one specific state each, but are characteristic for the distinction between the different states.[19] A division can be made between different types of phase-field variables: the first type, are solely introduced to avoid tracking the interfaces and are called phase-fields. This type describes which phases are present at a certain position in the system in a phenomenological way and is typically used for modelling solidification. The second type corresponds to well-defined physical order parameters, such as order parameters referring to crystal symmetry relations between coexisting phases, and composition fields.[4,14]

Another very common distinction in the phase-field variables can be made between either conserved or nonconserved variables. Conserved or composition variables can be mole fractions or concentrations. In a closed system with n components, n–1 mole fractions or concentrations (in combination with the molar volume) completely define the system, due to the conservation of the number of moles in a closed system. Nonconserved phase-field parameters can refer to the phases present, the crystal structure and its orientation. Because the variables are nonconserved, no restrictions are present on the evolution of the parameters as is the case for the conserved variables by the conservation of the number of moles. A distinction can be made between order parameters, referring to crystal symmetry relations between coexisting phases, and phase-fields, describing which phases are present at a certain position in the system in a phenomenological way.[4,14] In many applications of the phase-field model to real materials processes, it is often necessary to introduce more than one field variables or to couple one type of field with another. For example, in the case of modelling solidification, the temperature field T or concentration fields are coupled to the phase-field.[4]

1.2. Free energy description of the system

The possibility to reduce the free energy of the heterogeneous system is the driving force for microstructural evolution.[13,14] The selection of the thermodynamic function of state depends on the definition of the problem. An isolated, nonisothermal system, for example, requires a description based on entropy, whereas the Gibbs free energy is used for an isothermal system at constant pressure and the Helmholtz free energy is appropriate for a system with constant temperature and volume.[12] Phase-field models usually fix a certain volume to consider a certain system. Because the change in volume during transformations is small, the changes in Helmholtz free energy (defined for a constant volume) will deviate only slightly from the Gibbs free energy (defined for a constant pressure) and the changes in Gibbs and Helmholtz energy between 2 states are almost equal.[14]

In contrast to classical thermodynamics, where properties are assumed to be homogeneous, the phase-field method uses a functional of the phase-field variables and their gradients as a description for the free energy F of the system. The free energy density functional may depend on both conserved and nonconserved field variables, which are, in turn, functions of space and time.[11] Different driving forces for microstructural evolution (reduction in different types of energy) can be considered:[13,14]

$$F = F_{bulk} + F_{int} + F_{el} + F_{phys} \tag{1}$$

Where the bulk free energy, the interfacial energy, the elastic strain energy and an energy term due to physical interactions (electrostatic or magnetic) are present, respectively. The bulk free energy determines the compositions and volume fractions of the equilibrium phases.[13,14] The interfacial energy is the excess free energy associated with the compositional and/or structural inhomogeneities occurring at interfaces, of which the existence is inherent to microstructures.[4] The interfacial energy and strain energy affect the equilibrium compositions and volume fractions of the coexisting phases and also determine the shape and mutual arrangement of the domains.[13,14] The different contributions to the local free energy density are typically described by polynomials, of which the form is determined by the thermodynamic or mechanical model chosen to describe the material properties.[4,13,14] The coefficients in the polynomials become parameters of the model, which can be determined theoretically or based on experimental data.[13,14]

When temperature and molar volume are constant and there are no elastic, magnetic or electric fields, the total free energy of a system defined by a concentration field x_B and a set of order parameters η_k, is for example given by

$$F = \int [f(x_B, \eta, \vec{\nabla} x_B, \vec{\nabla} \eta_k)] dV = \int \left[f_0(x_B, \eta) + \frac{\varepsilon}{2} \left(\vec{\nabla} x_B \right)^2 + \sum_k \frac{\kappa_k}{2} \left(\vec{\nabla} \eta_k \right)^2 \right] dV \tag{2}$$

$f_0(x_B,\eta_k)$ refers to a homogeneous system where all state variables are constant throughout the system and is

called the homogeneous free energy density (J/m^3). For the nonconserved variables, it has minima at the values the variables can have in different domains. For the conserved variables, the homogeneous free energy density has a common tangent at the equilibrium compositions of the coexisting phases. $f(x_B,\eta_k,\nabla x_B,\nabla\eta_k)$ is the heterogeneous free energy density (J/m^3) and describes the heterogeneous systems, where the diffuse interfaces are present. A completely analogous expression is obtained when phase-field variables ϕ are used instead of the order parameters η_k.[14]

The gradient free energy terms $\frac{\varepsilon}{2}\left(\vec{\nabla}x_B\right)^2$ and $\frac{\kappa_k}{2}\left(\vec{\nabla}\eta_k\right)^2$ are responsible for the diffuse character of the interfaces: the homogeneous free energy f_0 forces the interfaces to be as thin as possible (due to the increase in energy with an increasing amount of material in the interface having nonequilibrium values), whereas the gradient terms force the interfaces to be as wide as possible (because the wider the interface, the smaller the gradient energy contribution due to the gentle change of the η_k value over the interface). Therefore, the equilibrium width of the diffuse regions is determined by two opposing effects.[2,14,20] $\boldsymbol{\varepsilon}$ and $\boldsymbol{\kappa}_k$ are called gradient energy coefficients and determine the magnitude of the penalty induced by the presence of the interfaces.[21] They are related to the interface energy and thickness.[14,20] Both terms, the gradient and the potential term, contribute in equal parts to the interface energy[17]

Typical expressions for f_0 are Landau polynomials of the fourth or sixth order in the phase-field and composition parameters. These expressions make use of the Landau theory of phase transformations. All the terms in the expansion corresponding to the local free energy density function are invariant with respect to symmetry operations.[20] For one order parameter (e.g., for simulating anti-phase domain structures) this could look like:

$$f_0(\eta) = 4(\Delta f_0)_{max}\left(-\frac{1}{2}\eta^2+\frac{1}{4}\eta^4\right) \tag{3}$$

Where $(\Delta f_0)_{max}$ is the depth of the free energy. $f_0(\eta)$ has double degenerate minima at −1 and +1, which could for example represent the two thermodynamically degenerate antiphase domain states. Note that only even coefficients are present in this polynomial, which finds its origin in the symmetry of the free energy expression around zero because both variants of the ordered structure are energetically equivalent. This expression only depends on one order parameter, but the Landau polynomial can also include compositional variables and order parameters.[4,13,14] For phase-field parameters, the homogeneous free energy typically contains an interpolation function f_p and a double-well function $g(\phi)$:

- The interpolation function f_p combines the free energy expressions of the coexisting phases in one expression by weighing them with a function of the phase-field parameter.

$$f_p(x_B,\phi,T) = (1-p(\phi))f^{\alpha}(x_B,T) + p(\phi)f^{\beta}(x_B,T) \tag{4}$$

The free energy expressions of the coexisting phases are usually constructed from thermodynamic data or assumed to have an idealized form. $p(\phi)$ should be a smooth function that equals 1 for $\phi = 1$ and equals 0 for $\phi = 0$ and $p'(\phi) = 0$ for $\phi = 1$ and $\phi = 0$. Mostly the following function is used (with g(ζ) representing the abovementioned double-well function):

$$p(\phi) = \frac{\int_0^{\phi} g(\zeta)d\zeta}{\int_0^{1} g(\zeta)d\zeta} = \phi^3\left(6\phi^2-15\phi+10\right) \tag{5}$$

Which satisfies $p(0) = 0$ and $p(1) = 1$ as well as $p'(\phi) = p''(\phi) = 0$ at $\phi = 0$ and 1. Another possibility for $p(\phi)$ could be:[22]

$$p(\phi) = \phi^2(3-2\phi) \tag{6}$$

- The double-well potential

$$g(\phi) = w\phi^2(1-\phi)^2 \tag{7}$$

has minima at 0 and 1 and w is the depth of the wells and can either be constant or depend on the composition. The double-well may be regarded as a term describing the activation barrier across the interface.[12] Another free energy function that is sometimes employed in phase-field models is the so-called double-obstacle potential,

$$f_0(\phi) = \Delta f\left(1-\phi^2\right) + I(\phi) \tag{8}$$

where

$$I(\phi) = \begin{cases} \infty, & |\phi| > 1 \\ 0, & |\phi| \le 1 \end{cases} \tag{9}$$

This potential has a computational advantage that, if the governing equations are solved in the neighborhood of the boundaries, the field variable assumes the value of −1 and +1 outside the interfacial region, because minimizing the free energy will make ϕ go steeper to its equilibrium value. This is in contrast with the case of the double-well potential (7), where the values of the field

variable slowly evolve to −1 and +1 away from the interface.[4]

2. Governing equations

The phase-field variables are functions of place and time and evolve toward a system with a minimal free energy functional. The temporal evolution of the variables is given by a set of coupled partial differential equations, one equation for each variable.[13,14] These equations ensure that the free-energy functional F decreases monotonically in time and guarantee local conservation of the conserved variables. The equations for microstructural evolution in variational phase-field models are derived based on general thermodynamic and kinetic principles, more specifically, they rely on a fundamental approximation of the thermodynamics of irreversible processes, i.e., that the flux describing the rate of the change is proportional to the force responsible for the change.[12,14] More information regarding nonequilibrium thermodynamics can be found in Refs.[16,23–25]

The generalized phase-field methods are based on a set of Ginzburg-Landau or Onsager kinetic equations.[11] The temporal and spatial evolution of conserved fields is governed by the Cahn-Hilliard equation, whereas the evolution of nonconserved fields is governed by the Allen-Cahn equation, also called the Ginzburg-Landau equation.[4,12] A thermodynamically consistent derivation of these equations is quite important, because it enables the correlation of the model parameters with each other, as well as the establishment of a sound theoretical background in thermodynamics.[17]

Several transport phenomena, besides diffusion, can have an effect on the microstructure, e.g., heat diffusion, convection and electric current. Using the formalism of linear nonequilibrium thermodynamics, it is straightforward to include these phenomena. However, extra equations will be required: modelling nonisothermal solidification uses the heat equation, whose kinetic parameter can be related to the thermal diffusivity; modelling convection in a liquid requires the combination of the phase-field equations with a Navier–Stokes equation, in which the viscosity depends on the phase-field variable.[14] Recently, the phase-field method was coupled with the lattice Boltzmann equation,[26–30] an alternative technique for simulating fluid flow. The next sections describe the two main types of governing equations (Cahn-Hilliard and Allen-Cahn) in more detail.

2.1. Ginzburg–Landau equation

The temporal evolution of the nonconserved order parameters and phase-fields is described by the Ginzburg–Landau or Allen-Cahn equation. Allen and Cahn[31] postulated that, if the free energy is not at a minimum with respect to a local variation in η, there is an immediate change in η given by

$$\frac{\partial \eta_k(\vec{r},t)}{\partial t} = -L_k \frac{\delta F}{\delta \eta_k(\vec{r},t)} \tag{10}$$

This equation expresses that the order parameter evolves proportional with the thermodynamic driving force for the change of that order parameter. The expression for this driving force is obtained with a thermodynamic approach: the dissipation of free energy as a function of time in an irreversible process must satisfy the inequality $\delta F/\delta t \leq 0$ as the system approaches equilibrium. When there are multiple processes occurring simultaneously, only the overall condition should be satisfied rather than the equation for each individual process. For example, an expansion of the general equation $\delta F/\delta t \leq 0$ gives:[12]

$$\left(\frac{\delta F}{\delta \eta_k}\right)_{c,T}\left(\frac{\partial \eta_k}{\partial t}\right)_{c,T} + \left(\frac{\delta F}{\delta c}\right)_{\phi,T}\left(\frac{\partial c}{\partial t}\right)_{\phi,T} + \left(\frac{\delta F}{\delta T}\right)_{\phi,c}\left(\frac{\partial T}{\partial t}\right)_{\phi,c} \leq 0 \tag{11}$$

Thus, with only a nonconserved order parameter as a variable, it is sufficient that[12]

$$\left(\frac{\delta F}{\delta \eta_k}\right)_{c,T}\left(\frac{\partial \eta_k}{\partial t}\right)_{c,T} \leq 0 \tag{12}$$

to ensure a monotonic decrease in the free energy of a system. Assuming that the flux is proportional with the force yields equation (10).[12] $\delta F/\delta \eta_k$ represents a variational derivative and applying the Euler–Lagrange equation[*32] yields[†]

$$\frac{\partial \eta_k(\vec{r},t)}{\partial t} = -L_k\left[\frac{\partial f}{\partial \eta_k} - \vec{\nabla}\frac{\partial f}{\partial \vec{\nabla}}\eta_k\right] = -L_k\left[\frac{\partial f_0}{\partial \eta_k} - \vec{\nabla}\cdot\kappa_k\vec{\nabla}\eta_k\right] \tag{13}$$

[*]The functional $A[f] = \int_{x_1}^{x_2} L(x,f,f')\,dx$ possesses an extremum for a function f that obeys the Euler–Lagrange equation:

$$\frac{\partial L}{\partial f} - \frac{d}{dx}\frac{\partial L}{\partial f'} = 0$$

[†]Note that most of the time, κ_k is assumed to be a constant and independent of the phase-fields. In such cases, the divergence of the gradient of the phase-field variable $(\vec{\nabla}\cdot\vec{\nabla}\eta_k)$ can be rewritten with a Laplace operator: $\Delta\eta_k = \nabla^2\eta_k$

In the single-phase-field model, an analogous expression is obtained:

$$\frac{\partial\phi(\vec{r},t)}{\partial t} = -L\frac{\delta F(x_B,\phi)}{\delta\phi(\vec{r},t)} = -L\left[\frac{\partial f_0(x_B,\phi)}{\partial\phi} - \vec{\nabla}\cdot\kappa(\phi)\vec{\nabla}\phi\right] \quad (14)$$

In phase-field models with more than two phases, multiple phase-fields ϕ_k are used to describe the phase fractions and therefore λ-multipliers or Lagrange-multipliers are used to ensure that all phase fractions sum up to 1 in every position of the system. L_k and L are positive kinetic parameters, related to the interface mobility (a measure for the speed at which the atoms can reorder from the original structure to the new structure).[14] $L_i = 1/\tau$, is the inverse of the relaxation time associated with how quickly the interface moves.[31]

2.2. Diffusion equations

The evolution of the conserved variables obeys a mass diffusion equation, which in turn is based on the continuity equation, stating that any spatial divergence in flux density must involve a temporal concentration change and taking into account mass conservation. It is based on linear non-equilibrium kinetics, according to which the atom flux is linearly proportional to the chemical potential gradient (the driving force for change in the composition). This chemical potential is actually the chemical potential difference between two species, i.e., that of the component under consideration and that of the dependent component.[33] If the free energy functional contains a gradient term for the conserved variable(s), this part of the energy functional is called the Cahn-Hilliard energy and the diffusion equation the Cahn-Hilliard equation. This type of kinetic equation can also be interpreted as a diffusional form of the more general Ginzburg–Landau equation.[11] The conserved variables evolve according to an equation of the form

$$\frac{1}{V_m}\frac{\partial x_B(\vec{r},t)}{\partial t} = -\vec{\nabla}\cdot\vec{J_B} \quad (15)$$

The diffusion flux $\vec{J_B}$ is given by

$$J_B = -M\vec{\nabla}\frac{\delta F}{\delta x_B} = -M\vec{\nabla}\left[\frac{\partial f_0(x_B,\eta_k)}{\partial x_B} - \vec{\nabla}\cdot\varepsilon\vec{\nabla}x_B(\vec{r},t)\right] \quad (16)$$

Parameter M describes the ease by which the atoms can move from one position to another and also determines the change in composition. The diffusion fluxes are defined in a number fixed reference frame, thus 'diffusion potentials' will refer to 'interdiffusion potentials' in the remainder of the text and the parameter M is related to the interdiffusion coefficient D as

$$M = \frac{V_m D}{\partial^2 G_m/\partial x_B^2} \quad (17)$$

The mobility coefficient can also be expressed as a function of the atomic mobilities of the constituting elements M_A and M_B, which in turn are related to tracer diffusion coefficients.[14] Mostly, the mobility coefficient is assumed to be independent of the composition, corresponding to dynamics controlled by bulk diffusion.

2.3. Thermal fluctuations

Stochastic Langevin forces are sometimes added to the right-hand side of each phase-field equation to account for the effect of thermal fluctuations on microstructure evolution. Moreover, because, except for the initial state of the system, the simulations are deterministic and although they can adequately describe growth and coarsening, they do not cover nucleation.[‡] To overcome this limitation, stochastic Langevin forces can be added, transforming the equations into:

$$\frac{\partial\eta_k(\vec{r},t)}{\partial t} = -L_k\frac{\delta F\left(x_B,\eta_j\right)}{\delta\eta_k(\vec{r},t)} + \xi_k(\vec{r},t) \quad (18)$$

$$\frac{1}{V_m}\frac{\partial x_B(\vec{r},t)}{\partial t} = \vec{\nabla}\cdot M\vec{\nabla}\frac{\delta F(x_B,\eta_k)}{\delta x_B(\vec{r},t)} + \psi_B(\vec{r},t) \quad (19)$$

With $\xi_k(\vec{r},t)$ nonconserved and $\psi_B(\vec{r},t)$ conserved Gaussian noise fields that satisfy the fluctuation-dissipation theorem. Mostly, the Langevin terms are used purely

[‡]As the density and spatial distribution of nuclei are critical in determining the phase-transformation kinetics and the resultant microstructure, which finally dictate the properties of the materials, one of the challenges in phase-field modelling is the simulation of the nucleation process. Governing equations in phase-field simulations are deterministic with the evolution of the phase-field variables toward the direction that decreases the free energy of an entire system. A nucleation event, however, is a stochastic event and may lead to a free energy increase. At the moment, two approaches exist to introduce nuclei within a metastable system: the Langevin noise method and the explicit nucleation method. The former incorporates Langevin random fluctuations into the phase-field equations. This reproduces the nucleation process well (with reasonable spatial distribution and time scale) when the metastable parent phase is close to the instability temperature or composition. When a system is highly metastable, on the contrary, it is difficult to generate nuclei with this method, because this yields an unrealistic large amplitude of noise, which can lead to over- or underestimated nuclei densities.[34]

The explicit nucleation method is based on the classical nucleation theory and the Poisson seeding. It incorporates nucleation ad hoc into the simulations. Separate analytical models that describe the nucleation rate and the growth of critical nuclei as a function of composition and temperature are used for this. Once a nucleus reaches the size of a grid spacing, it is included in the phase-field representation as a new grain, after which further growth is determined by the phase-field equations. Here, the following assumption is made: the time to nucleate a new phase particle is much shorter than the computational time interval Δt. This method has the disadvantage, however, that a sharp-interfaced nucleus is inserted into the system. This results in a relaxation of the compositional and phase-field variables around the newly inserted nucleus.[12,14,34]

to introduce noise at the start of a simulation and are switched off after a few time steps.[34] The presence of a noise term in the Cahn-Hilliard equation was also derived by Bronchart et al.[35] with a coarse grain method which was shown to lead to a rigorously derived phase field model for precipitation. These phase field equations are able to describe precipitation kinetics involving a nucleation and growth process.

3. Interfacial properties

In multiphase polycrystalline materials, interfaces are associated with structural and/or compositional inhomogeneities.[20] Interfaces are known as sites with an excess free energy, called the interfacial energy. In the phase-field model, the interfacial energy of the system is introduced by the gradient energy terms.[20] The properties of a flat interface between two coexisting phases are determined with the functional of the system energy, such as in (2).[36] The interface energy is defined by the difference per unit area of the system and that which it would have been if the properties of the phases were continuous throughout the system. It is given by an integral of the local free energy density across the diffuse interface region.[37] Thus, in the phase-field model, the interfacial energy contains two contributions: one from the fact that the phase-field variables differ from their equilibrium values at the interfaces and the other from the fact that interfaces are characterized by steep gradients in the phase-field variables. For some phase-field formulations, there exist analytical relations between the gradient energy coefficients and the interfacial energy and thickness.[4,37] Based on the definition of the interface energy (the difference between the actual Gibbs energy of the system with a diffuse interface and that containing two homogeneous phases each with their equilibrium concentration) and knowing that the equilibrium composition profile will be that which makes the interface energy minimal, yields a proportionality of the interface energy with $\sqrt{(\kappa(\Delta f)_{max})}$, where $(\Delta f)_{max}$ is defined as the maximum height of the barrier in the homogeneous free-energy density f between two degenerate minima.[37]

Moreover, the interfacial thickness should be defined, because in theory, a diffuse interface is infinitely wide.[37] One of the drawbacks of the phase-field method is that the simulations can be very computationally demanding. In real materials, the interfacial thickness ranges from a few Angstrom to a few nanometres.[12,14] To be able to resolve the interface and for numerical stability reasons, there must be at least 5–10 grid points in the interface in the simulations.[2] When using a uniform grid spacing and assuming the real interface width, this results in very large computational times (as the computational time scales with the interface thickness to the $-D$th power, where D is the dimension of the simulation, and furthermore, the largest possible time step is often, e.g., when an explicit time step is used, also largely reduced when Δx is decreased). It could also result in very small system sizes (of the order of 1 μm for two-dimensional systems and 100 nm for three dimensions). These dimensions are too small to study realistic systems and the phenomena therein.[12,14]

All the early models considered the diffusiveness of the interface as real and a property of the interface that can be predicted from the thermodynamic functional. A more pragmatic view, however, is that the diffuseness of the phase-field exists on a scale that is below the microstructure scale of interest. Thus its thickness can be set to a value that is appropriate for a numerical simulation.[17] Using a broader interface, reduces the computational resources required, but might also lower the amount of detail in the simulation. Adaptive grids might be a solution, as these have a finer grid spacing in the vicinity of the interface. But these are mostly a solution if the main part of the field is uniform and the interfaces only occupy a small part of the volume. It is, however, less useful in systems with multiple grains or domains.[12] This is why most phase-field simulations are applied in the 'thin-interface limit': interface widths are used as a numerical parameter and the interfaces are taken artificially wide to increase the system size, without affecting the interface behavior, diffusion behavior or bulk thermodynamic properties.[14] This is done by splitting the free energy density functional into an interfacial term and an independent chemical contribution and thus avoiding implicit chemical contributions to the interface energy which scale with the interface thickness.[38] The interface width is thus an adjustable parameter which may be set to physically unrealistic values, as is the case in most simulations.[12]

Here, the interface width is defined based on the steepest gradient (i.e., at the middle of the interface) so that an equal interface width results in equal accuracy and stability criteria in the numerical solution of the phase-field equations.[39] It is also important that the model formulation has enough degrees of freedom to vary the interfacial properties while the diffuse interface width is kept constant. In this way the movement of all interfaces is described with equal accuracy in numerical simulations.[37] Mostly, it is assumed that the interface width is proportional to $\sqrt{(\kappa/(\Delta f)_{max})}$, where $(\Delta f)_{max}$ is defined as the maximum height of the barrier in the homogeneous free-energy density f between two degenerate minima.[37] Thus, note that an increase in $(\Delta f)_{max}$ would increase the

interfacial energy but decrease the interfacial width, whereas an increase in κ, would yield both a decrease in the interfacial energy and in the interfacial width.[14]

4. Numerical solution methods

The microstructural and morphological evolution of the system is represented by the temporal evolution of the phase-field variables.[14] This temporal evolution of the phase-field variables is described by a set of partial differential equations, which are nonlinear and thus should be solved numerically, by discretization in space and time.[13,14,40] Several numerical methods exist, but most of them start with a projection of the continuous system on a lattice of discrete points. Then, the phase-field equations are discretized, yielding a set of algebraic equations. Solving these equations yields the values of the phase-field variables in all lattice points. The lattice spacing must be small enough to resolve the interfacial profile and the dimensions of the system should be large enough to cover the processes occurring on a larger scale. Note that a smaller lattice spacing will require a smaller time step to maintain numerical stability. The numerical solution methods can be subdivided into several categories: finite difference methods, spectral methods, finite element methods.

The simplest method is the finite difference discretization technique, also called Euler method, in which the derivatives are approximated by finite differences. Several types exist: forward, backward and central differences, depending on the 'direction' of the discretization step in space. A uniform lattice spacing is typically used. The partial differential equations in phase-field methods contain both derivatives with space and time, resulting in a discretization in both space and time. The discretization in time can be subdivided in two categories: implicit and explicit methods. The values of the variables at time step $n+1$ are directly calculated from the values at the previous time step n in the case of explicit time stepping. This is applied to the general evolution equation (20).

$$\frac{\partial \eta}{\partial t} = -L\left(\frac{\partial f_0}{\partial \eta} - \kappa \nabla^2 \eta\right) \tag{20}$$

Where η is the phase-field. In the two-dimensional case, the Laplacian operator can be discretized using a second-order five-point or a fourth-order nine-point finite-difference approximation. The five-point approximation at a given time step n for example

$$\nabla^2 \eta_i^n = \frac{1}{(\Delta x)^2} \sum_j \left(\eta_j^n - \eta_i^n\right) \tag{21}$$

Where Δx is the spatial grid size and j represents the set of first nearest neighbors of i in a square grid. The explicit finite-difference scheme can then be written as

$$\eta_i^{n+1} = \eta_i^n + \Delta t \left[\left(\frac{\partial f_0}{\partial \eta}\right)_i^n + \nabla^2 \eta_i^n\right] \tag{22}$$

A drawback of this method is the fact that the time step should be small enough for numerical stability, which results in long computation times. The time step constraint is dictated by

$$\Delta t \approx (\Delta x)^2 \tag{23}$$

When the Cahn-Hilliard equation, containing the biharmonic operator, is discretized, this square becomes a fourth power.[40] In contrast, implicit methods evaluate the right hand side of the discretized equation in (22) on time step $n+1$ instead of n, resulting in a set of coupled algebraic equations. This requires more intricate solution methods (linearization combined with iterative techniques), but it also allows for larger time steps.[41]

Spectral methods are a class of numerical solution techniques for differential equations. They often involve the Fast Fourier Transform. The solution of the differential equation is written as a sum of certain base functions, e.g., as a Fourier series, being a sum of sinusoids. The coefficients of the sum are chosen in such a way to satisfy the differential equation as well as possible.[41] One of these spectral methods is the Fourier spectral method with semi-implicit time stepping.[40] In this semi-implicit Fourier spectral method, the phase-field equations in real space are transformed to the Fourier space with a Fast Fourier Transformation. The convergence of Fourier-spectral methods is exponential in contrast to second order in the case of the usual finite-difference method. Transforming to the Fourier space, yields

$$\frac{\partial \tilde{\eta}(\vec{k}, t)}{\partial t} = -L\left(\widetilde{\frac{\partial f_0}{\partial \eta}}\right)_{\vec{k}} + (ik)^2 L\kappa \tilde{\eta}\left(\vec{k}, t\right) \tag{24}$$

Where $\vec{k} = (k_1, k_2, k_3)$ is a vector in Fourier space. k_1, k_2, and k_3 assume discrete values according to $\frac{l2\pi}{N\Delta x}$, where $l = -\frac{N}{2} + 1, \ldots, \frac{N}{2}$ with N the number of grid points in the system and Δx the grid space. A tilde ($\sim$) above a symbol refers to the corresponding Fourier transform of that symbol. The temporal derivatives are then differentiated semi-implicitly, i.e., the first term in (24) is evaluated at time step n, i.e., is treated explicitly, to reduce the associated stability constraint. Whereas the second term in the equation is evaluated at time step $n+1$, i.e., is treated implicitly, to avoid the expensive process of solving nonlinear equations at each time step. Solving a constant-coefficient problem of this form with the Fourier-spectral

method is efficient and accurate. However, periodic boundary conditions remain inherent to the method.

$$\frac{\tilde{\eta}^{n+1}-\tilde{\eta}^{n}}{\Delta t} = -L\left(\widetilde{\frac{\partial f_0}{\partial \eta}}\right)^{n}_{\vec{k}} - k^2 L\kappa\tilde{\eta}^{n+1} \tag{25}$$

This yields

$$\tilde{\eta}^{n+1} = \frac{\tilde{\eta}^{n} - \Delta t L\left(\widetilde{\frac{\partial f_0}{\partial \eta}}\right)^{n}_{\vec{k}}}{1+k^2 L\kappa\Delta t} \tag{26}$$

An inverse Fourier transform of the left hand side of (26) then gives η^{n+1} in real space. One benefit of this method is the fact that the Laplacian is treated implicitly, thus eliminating the need of solving a large system of coupled equations. Moreover, larger time steps can be used as compared to the completely explicit treatment, which would result in spectral accuracy for the spatial discretization, but the accuracy in time would only be of the first order. Thus a better numerical stability is associated with the semi-implicit method.[4,40] Moreover, a smaller number of grid points is required due to the exponential convergence of the Fourier-spectral discretization. Chen and Shen[40] demonstrated that, for a specified accuracy of 0.5%, the speed-up by using the semi-implicit Fourier-spectral method is at least two orders of magnitude in two dimensions, compared to the explicit finite difference-schemes (in the case of three dimensions, the speed-up is close to three orders of magnitude). Note that it is still only first-order accurate in time, but the accuracy in time can be improved by using higher-order semi-implicit schemes, i.e., also taking into account other time-steps than only the nth time step to determine the values in the $n+1$th time step. These higher-order semi-implicit schemes are, however, slightly less stable than lower-order semi-implicit schemes.[40]

Limitations of the method are the inherent periodic boundary conditions and the fact that the κ and L values are preferably constant to have the most efficient method. The latter may be circumvented by using an iterative procedure.[42,43] Another possibility was presented by Zhu et al.,[33] who imposed a compositional dependence on the mobility. They first transformed only the part after the second gradient in the Cahn-Hilliard equation. Then they applied the inverse Fourier transform on it, to multiply it afterwards with the mobility depending on the composition, because a multiplication in real space becomes a convolution in Fourier space. This entity was then transformed again to the Fourier space and then discretized semi-implicitly in time.

Because the spectral method typically uses a uniform grid for the spatial variables, it may be difficult to resolve extremely sharp interfaces with a moderate number of grid points. In this case, an adaptive spectral method may be more appropriate. It has been shown that the number of variables in an adaptive method is significantly reduced compared with those using a uniform mesh. This allows one to solve the field model in much larger systems and for longer simulation times. However, such an adaptive method is in general much more complicated to implement than uniform grids.[4]

Finite volume or finite element discretization methods are also used to solve phase-field equations.[14] Finite element methods are a class of numerical solution techniques for differential equations. Just like in the spectral methods, the solution of the differential equation is written as a sum of certain base functions, only this time the basic functions are not sinusoids but tent functions; it is also common to use piecewise polynomial basis functions. Thus, the main difference between both types of methods is that the basic functions are nonzero over the whole domain for spectral methods, while finite element methods use basis functions that are nonzero only on a small subdomain. Thus, spectral methods take a global approach, whereas finite element methods use a more local approach.

5. Quantitative phase-field simulations

The first phase-field simulations were qualitative with the limitation to observation of shape[12,17] and to obtain quantitative results one of the difficulties to overcome is the large amount of phenomenological parameters in phase-field equations.[14] The parameters are related to material properties relevant for the considered process. Ideally, the phenomenological description captures the important physics and is free from nonphysical side effects. The choice of the phenomenological expressions and model parameters, on the other hand, is somehow arbitrary and material properties are not always explicit parameters in the phenomenological model. Close to equilibrium, the model parameters can be related to physically measurable quantities[17]: the parameters in the homogeneous free energy density determine the equilibrium composition of the bulk domains; the gradient energy coefficients and the double-well coefficient are related to the interfacial energy and width; the kinetic parameter in the Cahn–Hilliard equation is related to diffusion properties and the kinetic parameter in the Ginzburg–Landau equation relates to the mobility of the interfaces.[14] The parameters may depend on the direction, composition and temperature. The directional dependence, in particular, determines the morphological

evolution.[14] Different methodologies can be applied to determine the missing parameters:

- Parameters that are difficult to determine for real materials can be approximated. For example, for the chemical energy part of the energy functional, for some materials, the temperature dependent description of Gibbs energies are available and can be directly used in the phase-field model. For a system with a limited thermodynamic database and when coarsening phenomena are considered, a parabolic function can be a good approximation of a real Gibbs energy function.[20]
- Measuring physical quantities that are linked to the phenomenological parameters. However, not every quantity is easy to determine: experimental information on diffusion properties, interfacial energy and mobilities is scarce. For example, measuring interfacial free energy of a material by direct experimental techniques is inherently difficult and relates mostly to pure materials,[14] but the presence of measurable quantities which are sensitive to the interfacial free energy developed indirect measurement techniques.[37]
- Reducing the dependence on experiments for this can be done by combining the phase-field method with the CALPHAD approach.[14] The CALPHAD (CALculation of PHAse Diagrams) method was developed to calculate phase diagrams of multicomponent alloys using thermodynamic Gibbs energy expressions.[14] Several software-packages can calculate phase diagrams and can optimize the parameters in the Gibbs energy expressions, e.g., Thermo-Calc[44] and Pandat.[45] DICTRA (DIffusion Controlled TRAnsformations) software[44] on the other hand, contains expressions for the temperature- and composition dependence of the expressions for atomic mobilities, obtained in a similar way as the Gibbs energy expressions in the CALPHAD method. The parameters are determined using experimentally measured tracer, interdiffusion, and intrinsic diffusion coefficients.[14]

  Coupling with these thermodynamic databases can retrieve the Gibbs energies of phases and chemical potentials of components.[14] Volume free energy densities are suitable for describing the total free energy functional. However, for evaluation of the chemical contribution in conjunction with thermodynamics databases, molar Gibbs free energy densities are preferred. Therefore, in most phase-field models, volume changes are neglected and the molar volumes of all the phases are assumed to be equal and are approximated to be independent of composition. In this way the volume free energy densities can be replaced by the molar Gibbs free energy densities ($f_0 = G_m/V_m$).[46] Moreover, $\partial G_m/\partial x_l = \mu_l - \mu_n$ (where n is the dependent component) which equals the diffusional chemical potential.
- The phase-field simulation technique can also be combined with ab initio calculations and other atomistic simulation techniques to obtain parameters that are difficult to obtain otherwise.[14,47] Ab initio calculations are based on quantum mechanics, i.e., solving the Schrödinger equation. For this some simplifying assumptions are required whenever multiple nuclei and electrons are present in the system. This method used to deliver mainly qualitative results 5 to 10 years ago regarding the relative stabilities of the crystal structure and is very promising as it requires almost no experimental input. Therefore, in theory, all parameters in the phase-field model can be calculated with an atomistic approach. Previously, the quantitative results from atomistic simulations themselves were not very reliable. There used to be large deviations, up to 200% or 300%, between values for the same properties calculated using different atomistic techniques or different approximations for the interaction potential.[14,47] However, the progress in this field has been enormous during the past decade. Computations with meV accuracy are nowadays possible and most of the commonly used codes and methods are now found to predict essentially identical results.[48] This allows to accurately predict phase stability and their coexistence. Wang and Li,[49] for example, give an overview of several studies using microscopic phase-field models with micro-elasticity and input from ab-initio as an alternative to the phase-field crystal method. This is another way to understand and predict fundamental properties of defects such as interfaces and dislocations and the interactions between dislocations and precipitates by using ab initio calculations as model input. These microscopic phase-field (MPF) models can predict defect size and energy and thermally activated processes of defect nucleation, utilizing ab initio information such as generalized stacking fault (GSF) energy and multi-plane generalized stacking fault (MGSF) energy as model inputs.

Furthermore, once the model is developed and if the role of each model parameter is understood, varying a parameter in different simulations and comparing the simulated microstructures with experimental observations can yield the proper value of the parameter.[37]

6. Historical evolution of phase-field models

6.1. First types of phase field models

It is generally accepted that Van der Waals[50] laid the foundations of the phase-field technique at the end of the 19th century by modelling a liquid–gas system with a density function that varied continuously over the interface. From general thermodynamic considerations he rationalized that a diffuse interface between stable phases of a material is more natural than the assumption of a sharp interface with a discontinuity in at least one property of the material.[17] In contrast, initial theoretical treatments of interfaces assumed two adjoining phases being homogeneous up to their common interface[51,52] or the existence of a single intermediate layer.[53,54] Another step in the right direction was taken by Rayleigh,[55] who noted the inverse proportionality between the interface tension and interface thickness. However, he did not take into account the increase in free energy due to the presence of nonequilibrium material in a diffuse interface and thus was not able to estimate the interfacial thickness. Others[56,57] were able to do the latter, but the calculations were based on the nearest neighbor regular solution model, making it less generally valid.

50 years ago, Ginzburg and Landau[58] proceeded on the ideas of Van der Waals[50] and used a complex valued order parameter and its gradients to model superconductivity.[11] Subsequently, Cahn and Hilliard[36] described diffuse interfaces in nonuniform systems by accounting for gradients in thermodynamic properties and even treating them as independent variables. This originated from the idea that the local free energy should depend both on the local composition and the composition of the immediate environment. The average environment that a certain region 'feels' is different from its own chemical composition due to the curvature in the concentration gradient.[12] As a result, the free energy of a small volume of nonuniform solution can be expressed as the sum of two contributions, one being the free energy that this volume would have in a homogeneous solution and the other a 'gradient energy' which is a function of the local composition.[36] A more mathematical explanation was also presented by a Taylor expansion limited to the first and second order terms. This expression was reduced to possess only even orders of discretization as the free energy should be invariant to the direction of the gradient. However, it is not clear to which extent his Taylor expansion remains valid.[12]

Cahn and Hilliard[36] also deduced a general equation to determine the specific interfacial free energy of a flat interface between two coexisting phases. The limitations of their treatment are the assumptions that the metastable free energy of the system must be a continuous function of the property concerned and that the ratio of the maximum in this free energy coefficient to the gradient energy coefficient should be small relative to the square of the intermolecular distance. If the latter condition is not fulfilled, there is a steep gradient across the interface and thus not only the second order derivatives should be taken into account in the Taylor series with respect to the gradient.

This method is quite similar to the one of Van der Waals.[50] This was discovered shortly after the publication of[36] by Cahn and Hilliard. In a second paper,[59] Cahn shows that their thermodynamic treatment of nonuniform systems is equivalent to the self-consistent thermodynamic formalism of Hart,[60] which is also based on the assumption that the energy per unit volume depends explicitly on the space derivatives of density. Hart defined all thermodynamic variables rigorously and related them uniquely with measurable variables. 20 years later, Allen and Cahn[31] extended the original Cahn-Hilliard model and described noncoherent transformations with nonconserved variables by the introduction of gradients of long-range order parameters into a diffusion equation. This is in contrast with the Cahn-Hilliard model, originally describing the kinetics of transformation phenomena with conserved field variables.[11] Thus, about a quarter of a century ago, these diffuse interface models were introduced into microstructural modelling. The term 'phase-field model' was first introduced in research describing the modelling of solidification of a pure melt[61–63] and nowadays, advanced metallurgical variants are capable of addressing a variety of transformations in metals, ceramics, and polymers.[11]

6.2. Solving free boundary problems with phase field models

The idea of using a phase-field approach to model solidification processes was motivated by the desire to predict the complicated dendritic patterns during solidification without explicitly tracking the solid–liquid interfaces. Its success was first demonstrated by Kobayashi[64] (and later by others[22]), who simulated realistic three-dimensional dendrites using a phase-field model for isothermal solidification of a single-component melt.[4] They developed a scheme to solve Stefan's problem of solidification of a pure substance in an undercooled melt by replacing the sharp interface moving boundary problem by a diffuse interface scheme.[17] The model which was originally proposed for simulating dendritic growth in a pure undercooled melt was extended to solidification modelling of alloys by a formal analogy between an isothermal binary alloy phase-field model and the nonisothermal phase-field model for a pure material.[65,66]

A number of phase-field models have been proposed for binary alloy systems and may be divided into three groups depending on the construction of the local free-energy functions.[4] The first is a model by Wheeler, Boettinger, and McFadden (WBM).[67] The second is a model by Steinbach et al.[19] and Tiaden et al.[68] The third type includes the models that are extensions of the models for pure materials by Losert et al.[69] and Löwen et al.[66]:

- The first type of phase-field models for solidification are of the type of the model by Losert et al.[69] This model has two unrealistic assumptions: the liquidus and solidus lines in the phase diagram were assumed to be parallel and the solute diffusivity is constant in the whole space of the system. These assumptions are clearly not generally true.[65]
- The WBM model is derived in a thermodynamically consistent way, as it guarantees spatially local positive entropy production.[67] The basic approach is to construct a generalized free energy functional that depends on both concentration and phase by superposition of two single-phase free energies and weighting them by the alloy concentration.[17] In the model, any point within the interfacial region is assumed to be a mixture of solid and liquid both with the same composition. Due to this fact that the compositions for all phases are the same, problems arise with the different phase diffusion potentials.[§12,46] Moreover, fictitious interfacial-chemical contributions are present which do not allow scaling of the interface width independently of other parameters.[38]

  The phase-field model of a binary alloy in WBM1 is based on a single gradient energy term in the phase-field variable ϕ and constant solute diffusivity. At first, solute trapping[**] was not observed in the limit under consideration: asymptotic analysis of the model in the limit of the sharp interface exposed a decrease in the concentration jump as a function of the velocity, as opposed to what is experimentally observed in the solute trapping effect. Therefore, subsequent work resulted in WBM2[70]: a phase-field model of solute trapping in a binary alloy that included gradient energy terms in both ϕ and c. This model could demonstrate solute trapping, but reconsideration of WBM1 showed that solute trapping can be recovered without the necessity of introducing a solute gradient energy term, but in a different limit than first considered.[71]
- The model by Steinbach et al.[19,68] uses a different definition for the free energy density: the interfacial region is assumed to be a mixture of solid and liquid with different compositions, but constant in their ratio, specified by a partition relation. Even though the derivation of governing equations in the model was not made in a thermodynamically consistent way, there is no limit in the interface thickness. The initial model was only thermodynamically correct for a dilute alloy.[65]

6.2.1. Decoupling interface width from physical interface width

For quantitative computations, the relationships between the model parameters and the material characteristics should be precisely determined in such a way that the interface dynamics of the PFM corresponds to that of the sharp interface in the corresponding free-boundary problem. A simple way to determine the relationships is to set the interface width in the PFM as the real interface width. In this case, however, the computational grid size needs to be smaller than the real interface width of about 1 nm. Mesoscale computations then become almost impossible because of the small grid size.[72,73] This stringent restriction of the interface width was overcome by Karma and Rappel's remarkable findings.[1]

They noted that the driving force is not constant if there is a significant concentration gradient on the scale of the interface width, as it depends on the local supersaturation and thereby on the concentration profile within the interface. Thus, Karma and Rappel[1] decoupled the interface width of the model from the physical interface width. They divided the driving force into two separate contributions: a constant part which represents the kinetic driving force acting on the atomistic interface, and a variable part that stems from the diffusion gradient in the bulk material apart from the atomistic interface.[17]

They showed that the dynamics of an interface with a vanishingly small width (classical sharp interface) can be correctly described by a PFM with a thin, but finite,

[§] $\tilde{\mu}_\alpha = \frac{\partial g_\alpha}{\partial c_\alpha}$ is here called *phase diffusion potential*, to distinguish it from the *diffusion potential* of the total phase mixture $\tilde{\mu} = \frac{\partial g}{\partial c}$, and from the *chemical potential* $\mu_\alpha = \frac{\partial G_\alpha}{\partial n_\alpha}$. Where g_α and G_α denote the chemical free energy density and the total chemical free energy of phase α, respectively; n_α denotes the number of moles in the solute component. This difference is illustrated in driving forces for solute diffusion and phase transformation: the gradient of phase diffusion potentials (for component i in phase α) $\nabla \tilde{\mu}_\alpha^i$ determines the driving force for solute diffusion, whereas the difference in chemical potential between the phases $(\mu_\beta^i - \mu_\alpha^i)$ is the chemical driving force for phase transformation.[46]

[**] Solute trapping occurs when a phase diffusion potential gradient exists across the diffuse interface.[65] A reduction is observed in the segregation predicted in the liquid phase ahead of an advancing front. The dependency of the jump in concentration on velocity of the interface is called solute trapping. In the limit of high solidification speeds, alloy solidification without redistribution of composition, not maintaining local equilibrium, is expected.[70] Thus, during rapid solidification, solute may be incorporated into the solid phase at a concentration significantly different from that predicted by equilibrium thermodynamics. In phase-field models, at low solidification rates, equilibrium behavior is recovered, and at high solidification rates, nonequilibrium effects naturally emerge, in contrast to the traditional sharp-interface descriptions.[71]

interface width if a new relationship between the phase-field mobility and the real interface mobility is adopted. To find the relationship between the phase-field parameters and the physical parameters in the sharp interface equation, a thin-interface analysis is required. In this analysis, an asymptotic expansion is executed and the surface is typically divided in an inner, outer and overlapping region. The solutions are written as expansions and in the matching region, the inner and outer solutions should describe the same solution. In thin-interface PFMs, the interface width needs to be much smaller than the characteristic length scales of the diffusion field as well as the interface curvature.[72] To obtain this, a phenomenological point of view is used: the phase-field variable is no longer used as a physical order parameter or density, but as a smoothed indicator function. The equilibrium quantities and transport coefficients are then interpolated between the phases with smooth functions of the phase-field variables.[74] Moreover, the interpolation function, which weighs the bulk energies of the different phases in the system, should satisfy certain conditions: it should be a smooth function equaling the correct values (i.e., -1, 0, or $+1$) in its minima and has a derivative that equals zero at these minima. Otherwise, the global minima of the energy functional of the system no longer lie at the proposed values of the phase-field variables. But these restrictions appear to be significantly less severe than those in previous PFMs, and the thin-interface PFM enables computation of the microstructure evolution on practical scales by ensuring correct behavior despite the presence of a diffuse interface between phases.[3]

6.2.2. Quasi-equilibrium condition

A second important development was implemented by Tiaden et al.[68] This model is actually an extension of the model of Steinbach et al.[19] The model of Steinbach et al.[19] did not include solute diffusion, but two years after the original model, Tiaden et al.[68] added solute diffusion to the multiphase model of Steinbach. The driving force for this solute diffusion was the gradient in composition and the diffusive law of Fick was solved in each phase. They assumed at any point within the interface a mixture of phases with different phase compositions, fixed by a quasi-equilibrium condition. In contrast to local equilibrium, this quasi-equilibrium condition assumes a finite interface mobility.[38] In the model of Tiaden et al.,[68] partition coefficients were used to model phases with different solute solubilities.

Kim et al.[65] showed later that the quasi-equilibrium condition is equivalent to the equality of the phase diffusion potentials for locally coexisting phases.[39,65] This is based on the assumption that the diffusional exchange between the phases is fast compared to the phase transformation itself.[38] By assuming that quasi-equilibrium is reached, the phase compositions can adjust instantaneously in an infinitesimally small volume, leaving the phase-fields and mixture compositions constant, but changing the diffusion potentials until a partial minimum of the local free energy is attained, i.e., to obtain a common value for the diffusion potential. This is the case if independent variation of the functional with respect to the phase compositions equals zero. This leads to the constraint that all phase diffusion potentials equal the mixture diffusion potential and thus also each other. Hence the term 'quasi-equilibrium', as the system does not necessarily need to be in equilibrium, even locally. During such phase transformations, diffusion potentials are locally equal, but the chemical potentials are still different from each other. Thus, the driving force for phase transformations remains present. This can be visualized by the parallel tangent construction (representing the equal diffusion potentials) (Figure 2 (b)) versus the common tangent construction (representing equal chemical potentials) (Figure 2 (a)).[46]

Kim et al.[65] developed a more general version of this type of phase-field model, usually abbreviated as the KKS model, for solidification in binary alloys by natural extension of the phase-field model for a pure material. They did this by direct comparison of the variables for a pure material solidification and alloy solidification and also derived it in a thermodynamically consistent way. At first, the model appeared to be equivalent with the Wheeler-Boettinger-McFadden (WBM1) model.[67] The WBM model, however, has a different definition of the free energy density for interfacial region and this removes the limit in interface thickness that was present in the WBM model. The interfacial region in the KKS model is defined as a mixture of solid and liquid with compositions different from each other, but with a same phase diffusion potential.[12,65] This is represented in Figure 3.

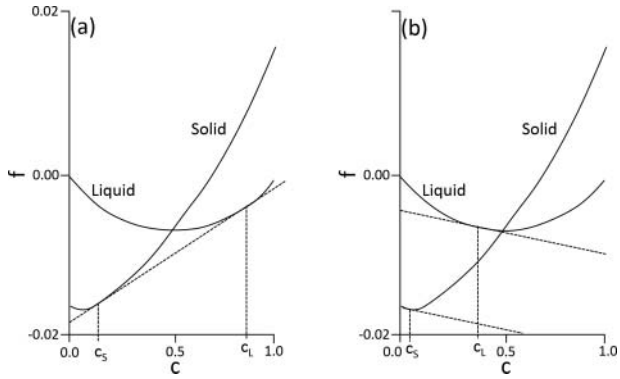

Figure 2. Representation of the parallel tangent (a) and common tangent (b) constructions.[67]

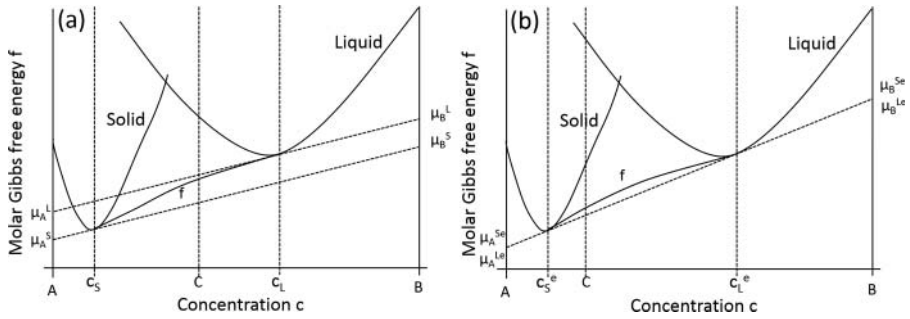

Figure 3. Molar Gibbs energy diagram for the phase-field model with the condition of equal diffusion potentials: nonequilibrium (a) and equilibrium (b) solidification. Under equilibrium conditions, the interface and bulk contributions are completely decoupled.[75]

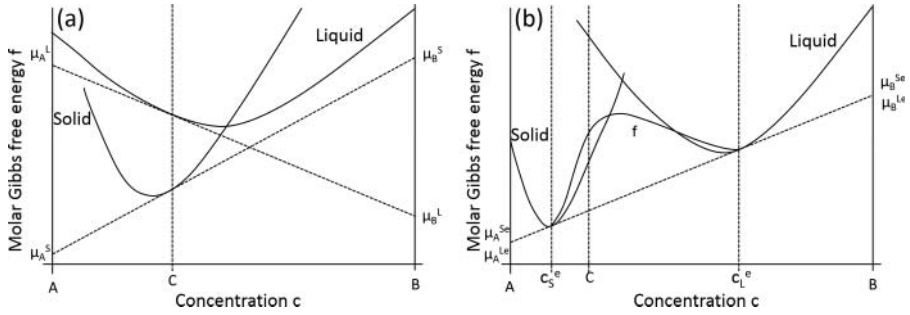

Figure 4. Molar Gibbs energy diagram for the phase-field model with the condition of equal concentrations $C_S = C_L = C$: nonequilibrium (a) and equilibrium (b) solidification.[75]

In the WBM model, on the contrary, the interfacial region was defined as a mixture of solid and liquid with a same composition, but with different phase diffusion potentials, as shown in Figure 4.[65]

Note that the condition of equal phase diffusion potentials in the KKS model does not imply the constant phase diffusion potential throughout the interfacial region. The phase diffusion potential varies across the moving interface depending on the position because the phase diffusion potentials are equal only at the same position. It is constant across the interface only at a thermodynamic equilibrium state. The phase diffusion potential can vary across the moving interface from the phase diffusion potential at the solid side to the phase diffusion potential at the liquid side of the interface, which results in the solute trapping effect, when the interface velocity is high enough. The energy dissipated by the boundary motion is called solute drag. In models, this solute drag is described as a fraction of the entire free-energy change upon solidification which is dissipated at the interface.[65,71]

Both the WBM and the KKS model were reformulated from the entropy or free energy functional or from thermodynamic extremal principles[††] by Wang et al.[75] Which definition for the interfacial region is more physically reasonable does not matter, because the interfacial region in PFMs cannot be regarded as a physical real entity, but as a mathematical entity for technical convenience.[65]

The solid curves in Figure 5 show typical free energy curves of solid and liquid as a function of the composition. The free energy density at the interfacial region in the WBM model lies on the red dotted curve and the chemical free energy contribution to the interface energy is graphically represented by the area under the free energy curves and the common tangent (PQ). The extra

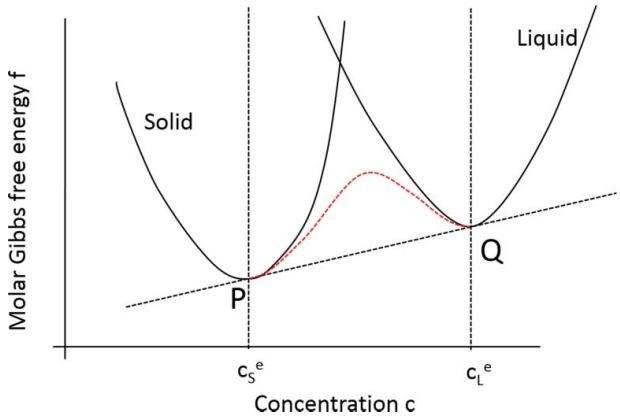

Figure 5. Free energy density curves of the individual phases (solid curves), of the WBM model (red dotted curve) and of the KKS model (dashed line PQ) as a function of concentration.[65]

[††]These include all the thermodynamic principles for modelling nonequilibrium dissipative systems, e.g., the Onsager's least energy dissipation principle, the maximal entropy production principle, etc.

potential in the WBM model may be negligible compared with $wg(\phi_0)$ either at the sharp interface limit where $w \to \infty$ or in an alloy with a very small c_L^e-c_S^e where the height of the extra potential itself is very small. With increasing interface thickness or increasing c_L^e-c_S^e, however, the extra potential height becomes significant and cannot be ignored. In the KKS model, on the other hand, the interfacial region at an equilibrium state is defined as a mixture of liquid and solid with constant compositions c_L^e and c_S^e, respectively and the excess energy in the interface region is removed by making the free energy equal to that of a two-phase mixture (i.e., the common tangent). The extra potential in the WBM model does not appear in the KKS model because the free energy is fraction-weighted after evaluation of the free energies of the phases in their respective equilibrium compositions, which corresponds to the common tangent line itself.[65]

The KKS model is reduced to the Tiaden et al.[68] model for a binary alloy at a dilute solution limit. Afterwards, Eiken (given name Tiaden) et al.[46] deduced the local quasi-equilibrium condition from a variational principle and showed again that it is equivalent to postulating equal diffusion potentials for coexisting phases. In summary, the thin-interface formulation combined with the quasi-equilibrium condition, used in the models of Tiaden et al.[46,68] and Kim et al.,[65] dictates, on the one hand, that, at each position, the diffusion potentials are equal in all phases and, on the other hand, that the bulk and interfacial energy were decoupled.[39] Imposing the equal phase diffusion potential condition upon the solid and liquid phases at a point of the system has two advantages over the traditional equal composition condition. The first is the relaxation of the restriction on the interface width in computation. The second is that the profile of the equilibrium phase-field gradient becomes symmetric.[72]

If instead of a free energy functional, a grand-potential ($\Omega = F - \mu N$) functional is used to generate the equations of motion, both types of abovementioned models can be obtained by the standard variational procedure. The dynamical variable is then the chemical potential instead of the composition and the driving force is the difference in grand potential. Here, the quasi-equilibrium condition is not required to be solved, and as the solution of these nonlinear equations in each point of the interface are computationally complex, a potentially large gain in computational performance is offered.[74] The extension of this model to multicomponent systems should be straightforward and was first roughly sketched in Ref.[76] Later, Choudhury and Nestler[77] performed this extension to multicomponent systems and proposed two methods, one implicit and one explicit, to determine the unknown chemical potentials. They benchmarked their calculations with the Al-Cu system and compared a phase-field model based on a free energy functional with a phase-field model based on a grand potential functional. They concluded that for finer microstructures resulting from high undercooling, both types of models approach each other, whereas at lower undercooling, the model based on the grand potential functional, can use larger interface widths.

6.2.3. Anti-trapping current term

The first step toward an improved (thin-interface) model was obtained by adopting the condition of equal diffusion potentials and finding a new relationship between the phase-field mobility and the real interface mobility with the thin-interface condition. However, this model still suffered from anomalous interface diffusion and/or an anomalous chemical potential jump at the interface which induces an exaggerated solute-trapping effect.[72] This chemical potential jump can be understood by looking into the composition profile around the interfacial region. Consider a one-dimensional solidifying system at instantaneous steady state with an interface velocity V in Figure 6. Assume that the interface width is sufficiently smaller than the diffusion boundary layer width in the liquid, that is, the thin-interface condition.[72]

There exist two straight parts in the profile of $c_{iL}(x)$. One is at the bulk solid side near the interface and the other at the bulk liquid side. These two straight parts can be extrapolated into the interfacial region, as shown by the dashed lines. Then the dynamics of the diffuse

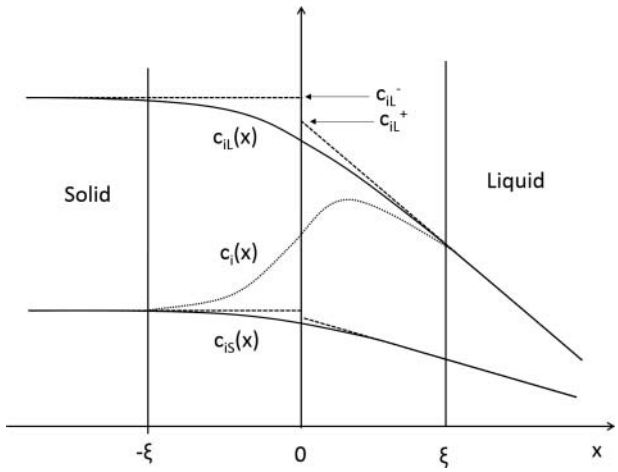

Figure 6. Composition profiles across the interface $-\xi < x < \xi$. The composition profile $c_{iS}(x)$ of ith solute in the solid, $c_{iL}(x)$ in the liquid and the mixture composition $c_i(x)$ are denoted by the lower thick curve, the upper thick curve and the dotted curve, respectively. The origin ($x = 0$) was defined as the position with $\varphi = 0.5$. The dashed lines are the extrapolations of the linear parts in $c_{iS}(x)$ and $c_{iL}(x)$ into the interfacial region.[72]

interface with the composition profiles of the thick curves represents effectively that of the classical sharp interface with the composition profiles of the dotted lines. These two extrapolated lines from the solid and liquid sides intersect the vertical axis at $c_{iL} = c^{-}{}_{iL}$ and $c_{iL} = c^{+}{}_{iL}$. For an interface with a finite width, there exist a finite difference between $c^{-}{}_{iL}$ and $c^{+}{}_{iL}$. This yields a corresponding difference in chemical potential, which has been called the chemical potential jump.[73,78] These anomalous interface effects become significant with increasing interface width in the simulation. Even though each of the anomalous interface effects can be effectively suppressed by adopting the relevant interpolation function with a specific symmetry, not all of them can be suppressed simultaneously.[72] Thus, quantitative modelling is not possible. Therefore, the addition of a nonvariational anti-trapping current became necessary, to decouple bulk and interface kinetics: all the anomalous interface effects could be suppressed by introducing an anti-trapping current term into the diffusion equation which acts against the solute-trapping current driven by the phase diffusion potential gradient and eliminates simultaneously all the interface effects. This was introduced by Karma[73] for dilute binary alloys with $D_S << D_L$ (i.e., a one-sided model zero diffusivity in the solid[15]) and worked out by Echebarria et al.[78] and Ramirez et al.[79] for binary dilute alloys with negligible diffusion in the solid, yielding quantitative simulations of alloy solidification. These were later extended to also model alloy solidification in multiphase[80,81] and multicomponent alloys.[72] These models are, however, introduced in a nonvariational way.[82]

The anti-trapping current is a compensation of the asymmetric fluxes in the interfacial region if the diffusivity differs a lot in the two phases and equals $j_A^i = A^i \dot{\phi} \vec{n}$. The trapping function A^i will be determined by the condition of a vanishing potential jump.[17,39] The anti-trapping current is nonvanishing only in the diffuse interface region. It produces a solute flux from the solid to the liquid along the direction normal to the interface that counterbalances the trapping current associated with the jump of phase diffusion potential across the interface. This current makes it possible to eliminate the jump, while leaving enough freedom to choose the other functions in the model to eliminate the modifications to the mass conservation conditions (interface stretching and surface diffusion).[73]

Following Karma's finding, two similar methods were proposed independently. Both methods are based on the fact that all the anomalous interface effects originate from the finite interface width in the diffusion equation, not in the phase-field equation. The anomalous interface effects can then be suppressed by decoupling the interface width in the diffusion equation from the width in the phase-field equation and taking the limit that the width in the diffusion equation goes toward 0. The other possibility is the anti-trapping PFM, where the solute-trapping phenomenon can be controlled independently of the grid size. Anti-trapping PFMs were first limited to binary dilute alloys, until Kim[72] extended this to nondilute multicomponent alloys. This model was restricted to solidification into a single solid phase. Solidification of useful multicomponent alloys often accompanies two or more solid phases. Recently Folch and Plapp[81] developed an anti-trapping PFM for eutectic solidification where two solid phases form simultaneously from a liquid phase. They used a smooth free-energy functional with a parabolic form for the chemical energy which ensured the absence of any third phases in the interfaces and eliminated all thin-interface corrections to the desired free-boundary dynamics. Their model is, however, restricted to dilute binary alloys. Kim[72] later extended the anti-trapping PFM further to multicomponent systems with arbitrary thermodynamic properties. Recently, several extensions of the anti-trapping current were put forward to generalize the approach to the case of finite diffusivity in the solid.[83,84] The former simulations are done for a planar interface[83] and the latter for free dendritic growth,[84] which show that the approach works well.

Another completely variational approach was taken by Brener and Boussinot:[82] they developed a phase-field model for isothermal transformations that includes Onsager kinetic cross coupling between the conserved and nonconserved variables. As the classical variational formulations of the evolution equations is of a diagonal form, i.e., the change of one variable in time only depends on the functional derivative of the free energy with respect to that same variable and not the other variable present in the system description, they introduced kinetic cross coupling into the phase-field equations with a nondiagonal formulation. This resulted in a term ($M_C W \dot{\phi} \nabla \phi$) in the diffusive equation with the same shape as the anti-trapping current (where $\nabla \phi$ is used as a vector normal to the interface) mentioned above, but now it is obtained in a variationally derived phase-field model. Moreover, another term also appears in the equation describing the evolution of the nonconserved variable. This model was limited to a two-component system with only two phases.

6.2.4. Finite interface dissipation

It is not clear at what point the assumptions of irreversible thermodynamics, on which the equations describing microstructural evolution are based, would fail. Furthermore, the usual phase-field framework is not well suited for the description of strong nonequilibrium effects

because the equations for interface motion are often obtained by a Taylor expansion around the equilibrium solution, which is formally valid only for small driving forces. Moreover, little is known about the initial stage when the two materials are far from common equilibrium. This is in contrast with the abovementioned quasi-equilibrium models, which assume equal diffusion potentials from the start of the simulation.[85]

For two materials, with certain initial compositions, in contact, these compositions are, generally, out of equilibrium, i.e., the chemical potentials do not coincide. As soon as a common interface is formed, its composition can change. It is a plausible assumption that the interface composition should lie somewhere between the initial compositions of the two phases. However, it is not possible to determine the interface composition based on thermodynamics, since thermodynamic equilibrium is not present in the system and the problem is actually a kinetic one.

Galenko and Sobolev[86] investigated nonisothermal rapid solidification of undercooled alloys, which can be so fast that the interface velocity is an order of magnitude faster than the diffusive speed. Thus, the solute flux cannot be described by the classical mass transport theory and they took the deviations from local equilibrium into account in the phases, which affect both the diffusion field and the interface kinetics. By using Fick's generalized law for local nonequilibrium diffusion, which takes into account the relaxation to local equilibrium of the solute flux, they obtained a hyperbolic equation for the solute concentration.

Later, Lebedev et al.[87] generalized this theory by introducing a nonequilibrium contribution to the free energy density which takes into account the relaxation of the flux to its steady state and the rate of change of the phase field. In the limit of instantaneous relaxation, this contribution disappears. The requirement that the free energy decreases monotonically during the relaxation of the system toward equilibrium, leads naturally to hyperbolic evolution equations. Using this hyperbolic extension of the WBM model, they were able to construct kinetic phase diagrams to investigate solute trapping for Si-As alloys. It became clear that the actual interval of solidification shrinks with increasing interface velocity. The model considered ideal solutions and only 1-D phase-field simulations were performed.

Steinbach et al.[85] later developed a phase-field model with finite interface dissipation, but based on their previous model with equal diffusion potentials[19,68] instead of the WBM model used by Galenko and Sobolev[86] and Lebedev et al.[87] In practice, this means that the 'static' quasi-equilibrium condition is replaced by a kinetic equation that drives the concentration fields to the desired equilibrium. Such a kinetic equation is not solved for the global concentration, but for the phase compositions. The point of solving these equations separately avoids the need to employ an extra condition to fix the concentrations for each phase. Instead, the separated concentration evolution equations of each phase can be used for the iteration in time. For slow kinetics or rapidly moving interfaces, a difference between the chemical potentials in the two phases appears naturally. This difference in chemical potentials can be controlled by the rate constant of the kinetic equation, which is called the interface permeability and which can be used to tune the interface dissipation. The model naturally recovers the model with equal diffusion potentials (high permeability / fast exchange), solute trapping and phase transformations out of diffusion control.[85]

Later, Zhang and Steinbach also extended this model to become applicable to multicomponent multiphase alloys.[88] The formulation is proposed in two different models. In model I, the overall mass conservation between the phases of a multiple junction is used, whereas, in model II, the concentrations of each pair of phases have to be conserved during the transformations. Both models demonstrate the decomposition of the nonlinear interactions between different phases into pairwise interaction of phases in multiple junctions. Both models converge to the same equilibrium state while in nonequilibrium states they differ.

Later, Wang et al.[89] used the maximal entropy production principle to develop a model for rapid solidification in binary alloys. In this way, the mobility for the exchange process or the 'interface permeability' does not need to be defined to determine the Langrangian multiplier used by Steinbach et al.[85,88] They applied the model to a Si – 9at% As alloy and the simulated solute trapping showed good agreement with experimental results for various velocities. However, the model was still of a parabolic nature and thus only applicable in theory to solidification with slow dynamics, characterized by a growth velocity much smaller than the maximal solute diffusion velocity in the bulk phases, resulting in a situation with only the interface in nonequilibrium.

To fully describe nonequilibrium solute diffusion, considering not only the interface but also the bulk phases out of equilibrium, Wang et al.[90] proposed a hyperbolic phase-field model from the thermodynamic extremal principle. The solute diffusion then splits in long-range solute diffusion and short-range solute redistribution between the two phases. In this model, however, the transition from diffusion-limited to diffusionless solidification shows a gradual disappearance of solute drag as the velocity of the interface reaches infinity. However, sharp interface models with local nonequilibrium effects show a critical velocity after which

solute drag abruptly stops to be present which concurs with the transition to diffusionless solidification. Thus, Wang et al.[91] used an effective mobility approach instead of the previous kinetic energy approach for nonequilibrium solute diffusion. The effective mobility approach does not only result in an extra kinetic energy term to the free energy density, according to the kinetic energy approach, but the kinetic mobility for solute diffusion was also changed from its usual definition connecting it with the diffusion coefficient, to an effective definition, also taking into account the solute speed at the interface. This model for binary alloys was later extended to multiphase systems by Zhang et al.[92] They applied the model to the nonequilibrium solidification of Al-Si-Cu alloys, which showed that anomalous solute trapping can take place if the interaction among the component elements is strong enough.

6.3. Multiphase-field models

Early phase-field models for a three-phase change problem, were developed for eutectic systems and consisted of a dual phase-field model (for solid and liquid) superposed by a Cahn–Hilliard model for demixing in the solid. Thus, they were restricted to a three-phase transformation. To be applicable to an arbitrary number of different phases or differently oriented grains of the same phase, multiphase-field models were developed.[17]

First, Steinbach et al.[19] developed a multiphase-field model, where each phase is identified with an individual phase-field and the transformation between all pairs of phases is treated with its own characteristics. The free energy functional describing the system is actually an expansion in a series over the pairwise interaction energies between the different phases. Tiaden et al.[68] extended this model to also account for diffusion in multiphase systems and to describe the evolution of the microstructure during solidification processes in alloy systems. They used this model to compute the peritectic solidification process of steel. The free energy functional of the system is described by equation (27).

$$F\left(x_\alpha^i,\phi_k\right)=\int\left[\sum_{\beta=1}^{p}\sum_{\alpha=1}^{\alpha=\beta}\frac{1}{2}\varepsilon_{\alpha\beta}\left(\phi_\alpha\vec{\nabla}\phi_\beta-\phi_\beta\vec{\nabla}\phi_\alpha\right)^2+\frac{1}{a_{\alpha\beta}}\phi_\alpha^2\phi_\beta^2-m_{\alpha\beta}\left(\frac{1}{3}\phi_\alpha^3+\phi_\alpha^2\phi_\beta-\frac{1}{3}\phi_\beta^3-\phi_\beta^2\phi_\alpha\right)\right]dV \tag{27}$$

$\varepsilon_{\alpha\beta}$ is the gradient energy coefficient and $1/a_{\alpha\beta}$ is proportional to the pairwise energy barrier height. The driving force for the phase transition between the phases α and β is defined by the deviation from the two phase equilibrium and is described by $m_{\alpha\beta}$.[68] The first term in (27) is the kinetic term, obtained from an expansion in a series over powers and considering aspects of symmetry. This term can be interpreted as follows: the gradient of one order parameter $\nabla\ \phi_\alpha$ measures the interface energy to all the rest of the phases. The contribution of one specific interface type $\phi_\beta \rightarrow \phi_\alpha$, therefore, is weighted by the density of these states. $\nabla\ \phi_\beta$ has no contribution to the phase transformation $\phi_\beta \rightarrow \phi_\gamma$, if $\phi_\gamma = 0$ in the local volume, i.e., if no phase ϕ_γ is present. The operator $\phi_\alpha\nabla\ \phi_\beta - \phi_\beta\nabla\ \phi_\alpha$ fulfils this requirement to the lowest order ϕ_β and $\nabla\ \phi_\beta$. The last two terms in (27) represent the potential part of the local free energy and are a direct extension of the standard double well function, this is called a multiwell potential and is characterized by the proportionality to $\phi_\beta{}^2\phi_\alpha{}^2$ instead of the proportionality to $\phi_\beta\phi_\alpha$ that would be the case for the multi-obstacle potential. The pair potential contributions ($\phi_\beta\phi_\alpha{}^2$, $\phi_\beta{}^2\phi_\alpha$ and $\phi_\beta{}^2\phi_\alpha{}^2$) are nonzero only at the interface and define the potential barrier between both phases to prevent spontaneous phase transitions.[19]

As the phase-fields should sum up to be one, the phase-fields are not independent field variables, yielding nonlinearities, which were originally attributed to triple point energies and energies of multiple interactions of higher order. Moreover, the physical assumption was made that these triple point energies and energies of multiple interactions of higher order have negligible influence on the total energy of the system and thus the corresponding nonlinearities were neglected. This approximation, however, was shown[93] to violate the conservation of interfacial stresses at multiple points. Thus, the torque terms should be taken into account as the multiple phase energies will influence the local physics significantly.[94]

Both the models of Steinbach et al.[19] and Tiaden et al.[68] are applicable for binary alloys, but not for systems with more components, which is more common in practice. The model by Eiken et al.[46] is an extension for multicomponent systems of the multiphase-field model and is based on those of Tiaden et al.[68] and Steinbach et al.[19] Moreover, Eiken et al.[46] reformulated the model in an almost thermodynamically consistent form and derived the governing equations and the local quasi-equilibrium constraint from the free energy functional with variational principles. These systems with more than two coexisting phases are mainly used to simulate grain growth.[4,68] In a multiphase-field model, p phase-fields ϕ_k (comprised in a vector) describe the p coexisting phases. The phase-fields represent the local fractions of the different phases and thus should sum up to one at every point in the system. The free energy as a functional of the molar fractions $x_i(r,t)$ and phase-fields $\phi_k(r,t)$ can be split into the chemical and the interface free energy

density and has the form[19,46]:

$$F\left(x_\alpha^i,\phi_k\right)=\int f^{chem}\left(x_\alpha^i,\phi_k\right)+f^{intf}\left(\phi_k\right)dV$$
$$=\int\left[\sum_{\alpha=1}^{p}\phi_\alpha f_\alpha\left(x_\alpha^i\right)+\sum_{\alpha,\beta=1}^{p}\frac{4\sigma_{\alpha\beta}}{\eta_{\alpha\beta}}\left[-\frac{\eta_{\alpha\beta}^2}{\pi^2}\nabla\phi_\alpha\cdot\nabla\phi_\beta+\phi_\alpha\phi_\beta\right]\right]dV \tag{28}$$

where $\sigma_{\alpha\beta}$ is the interface energy between phase α and phase β in a multiphase junction with p phases or differently oriented grains and $\eta_{\alpha\beta}$ is the interface width. A double obstacle potential is used. The chemical part of the free energy density functional is formulated as the sum of the free energy densities of the individual phases f_α weighed by the respective phase-fields (i.e., the phase fractions). Note that the free energies of the individual phases depend on individual phase compositions x_α^i, which are constant over an interface in equilibrium, in contrast to the continuous mixture composition variables x_i. The phase compositions are nonconserved, whereas the global compositional variables are.[46]

Moreover, due to the weighing of the free energies of the individual phases with the respective phase fractions, the following relation between the phase diffusion potentials and the (mixture) diffusion potential is found:[46]

$$\tilde{\mu}^i=\sum_{\alpha=1}^{p}\phi_\alpha\sum_{j=1}^{n}\tilde{\mu}_\alpha^j\frac{\partial x_\alpha^j}{\partial x_i} \tag{29}$$

Assuming quasi-equilibrium, an independent variation of the functional with respect to the phase compositions should equal zero. This leads to the constraint that all phase diffusion potentials equal the mixture diffusion potential and thus also each other.[46] A more general approach weighs the free energy densities of the individual phases with an interpolation function that should be smooth and equals 1 where the corresponding phase-field equals 1, and equals 0 where the corresponding phase-field equals 0.[19] Afterwards, Carré et al.[95] formulated a general expression for the anti-trapping current in such a multicomponent multiphase-field model with a double obstacle potential, based on the approach proposed by Kim.[72] The anti-trapping correction is needed when the diffusivity in one phase can be considered negligible, whereas, if the diffusivities in both phases are equal, no corrections are required.

A problem of the abovementioned multiphase-field formalism is that the exact dynamics of multiple junctions are not represented correctly: a third phase may appear at the interface between two phases, which affects the interfacial properties and complicates parameter assessment. This finds its origin in the third term of the most right-hand side of (28): the diffusive terms are weighted with the phase-field variables of the counter phase, to concentrate the thermodynamic driving force to the center of the interface. These equations cannot be derived rigorously from a free energy formulation and may thus violate the energy balance at triple junctions.[46]

Efforts were made to find formulations that reduce or avoid this unphysical third-phase effect. A multi-obstacle potential can diminish the interference of third phases at two-phase interfaces ('ghost phases') as it suppresses the spreading out of multiple junctions into the interface region. In contrast, the double well potential is cubic in the phase-field variable, which energetically favors multiple junctions. For the double well, the growth of the third phase reduces the potential energy and the dual interface becomes intrinsically unstable. Thus, a strong counter-energy is needed to suppress spreading out of the multiple junctions into the interface region. The use of a double- or multi-obstacle potential also reduces to a certain extent the artificially large interaction between neighboring particles.[46] Only solving the equations at the interfaces would also be possible, but is sometimes combined by just putting the 'extra' phase-field equal to zero when it appears after a certain number of time steps in the simulations, making it a questionable method. Alternatively, higher-order terms $\propto \phi_i\phi_j\phi_k$ can be used with high factors in front of them.[96] But it remains unclear what the influence of the latter is on triple junctions, which are not unphysical in nature.[14]

Moreover, another general problem arose: the interpolation functions for two-phase systems do not extend to multiphase systems.[17,39] The interpolation functions should have zero slope at the equilibrium values of the nonconserved variables representing the different phases, should allow for a thermodynamically consistent interpolation of the free energies and thus be suitable for multiple junctions and cannot violate the sum constraint $\sum \alpha = 1,..,N\, h(\phi_\alpha) = 1$.[17,39]

For example $h(\phi) = \phi^3\ (10 - 15\phi + 6\phi^2)$ is frequently used as an interpolation function in a solid–liquid system, but does not generalize to multiphase systems. Generalizing to multiphase models with $\phi_i = 1$ and $\phi_j = 0, \forall\, j \neq i$ representing phase i and $\sum\phi_i = 1$, would give a bulk free energy of the form $f_b = \sum h_i(\phi_i)\, f$. Which, without extra constraints for $h_i(\phi_i)$, is thermodynamically inconsistent since $\sum h_i(\phi_i) \neq 1$ and this will result in energy generation in multijunctions. Thus, even though an interpolation function of the form $h_i(\phi_i) = \phi_i$ is often used in multiphase-field models, this shifts the local minima of the total free energy, resulting in difficult-to-control inaccuracies.[39]

Folch and Plapp[81] formulated a free energy functional for systems with three phases with polynomials of the fifth-

order in the phase-fields as interpolation functions. These interpolation functions allow for a thermodynamic consistent interpolation between the free energies of the three coexisting phases and keep the local minima of the free energy at the intended positions. A generalization to multiphase systems, however, was unfeasible, as the order of the interpolation polynomial has to increase with the number of phases to maintain satisfying all requirements for a quantitative phase-field model.[39] Multi-order parameter representations are also possible, but do not extend to multiphase models, as they do not require the order parameters to sum up to one, as the phase-field variables in a multiphase-field model. Moelans[39] introduced a new type of interpolation function for quantitative phase-field modelling for multiphase systems. The interfacial free energy for polycrystalline structures introduced by Moelans et al.[37,97] was extended to multiphase systems and a bulk free energy was derived, starting from the thin-interface approach of Tiaden et al.[46,68] and Kim et al.,[65] but using a different type of interpolation function between the free energies of the different phases:

$$f_b = \sum_{ip} h_{ip} f_{ip}\left(x_1^{ip}, \ldots, x_k^{ip}, \ldots, x_{C-1}^{ip}\right) \tag{30}$$

The interpolation functions h_{ip} must have a zero slope at the equilibrium values of the nonconserved phase-fields or order parameters representing the different phases and $\sum h_{ip}$ must equal 1. Moreover, due to the quasi-equilibrium condition, the phase diffusion potentials of all components should be equal in all coexisting phases:

$$\tilde{\mu}_k = \frac{\partial f_{1p}(x_k)}{\partial x_k^{1p}} = \ldots = \frac{\partial f_{np}(x_k)}{\partial x_k^{np}}, \qquad \forall\ k \tag{31}$$

And the overall composition of a component k should relate to the phase compositions as

$$x_k = \sum_{ip} h_{ip} x_k^{ip} \tag{32}$$

An important advantage of this approach compared to other quantitative alloy approaches is that composition-dependent Gibbs energy expressions for multicomponent systems optimized according to the CALPHAD approach can be used directly in the phase-field bulk energy in equation (30). Moelans introduced the following interpolation function for these multiphase systems:[39]

$$h_{ip} = \phi_{ip} = \frac{\eta_{ip}^2}{\sum_{ip=1p}^{np} \eta_{ip}^2} \tag{33}$$

Note the change in notation: η_{ip} now represents the phase-field variable and ϕ_{ip} represents the phase fraction. Typically, $\sum_{ip=1p}^{np} \eta_{ip} \neq 1$. In this model, the interfacial free energy functional is represented by:

$$f_s = m f_0(\eta) + \frac{\kappa(\eta)}{2} \sum_{\rho} \sum_{i=1}^{p_\rho} \left(\vec{\nabla} \eta_{\rho i}\right)^2 \tag{34}$$

With f_0 a fourth order Landau polynomial of the order parameters:

$$f_0(\eta) = \sum_{\rho} \sum_{i=1}^{p_\rho} \left[\frac{\eta_{\rho i}^4}{4} - \frac{\eta_{\rho i}^2}{2}\right] + \sum_{\rho} \sum_{i=1}^{p_\rho} \left[\sum_{\sigma} \sum_{j=1, \rho i \neq \sigma j}^{p_\sigma} \frac{\gamma_{\rho i, \sigma j}}{2} \eta_{\rho i}^2 \eta_{\sigma j}^2\right] + \frac{1}{4} \tag{35}$$

Which is based on the model of Chen and Yang[6] for normal grain growth in pure single-phase materials. Each term in the first set of summations is a double-well potential with minima located at -1 and $+1$ for $\eta_{\rho i}$. The cross terms ($\gamma_{\rho i, \sigma j} \eta_{\rho i}^2 \eta_{\sigma j}^2$) were added to make it energetically unfavorable to have two order parameters different from zero at the same position in the system because it gives a positive contribution to the local free-energy density for each extra phase-field variable with a value different from 0. By consequence, within the grains only one of the phase-field variables differs from 0 and at a grain boundary and multijunctions, only those phase-field variables representing the adjacent grains are different from zero.[37,98]

Both the multiphase-field (MPF) type of models, based on the approach of Steinbach et al.,[19,46,68] and the continuum field (CF) models, based on the approach of Chen and Yang,[6] are still used in phase-field modelling. A major distinction between those two types of phase-field models is in the interpretation of the phase-fields. In continuum field models, the field variables are treated as being independent. At the diffuse grain boundaries, the variables change monotonously between values without any constraint. In multiphase-field models, in contrast, the phase-fields are interpreted as volume fractions which therefore are subject to the constraint that the sum of the phase-fields must be equal to one at each position in the system. Furthermore, the thermodynamic free energy in the continuum field

model has multiple degenerate minima, one for each grain orientation. The free energy of the multiphase-field model has a single minimum for all phase-fields equal to zero. It is the constraint on the sum of the phase-fields that forces one of them to equal 1 within the grains.

Moelans et al.[99] compared both types of models in the context of grain growth and derived relationships to obtain equivalent parameters in both types of models. The advantage of the MPF model is that most parameters are directly related to physical quantities, whereas it requires the numerical calculation of an integral to relate the model parameters in the CF model to physical quantities. In the MPF model, on the other hand, third-order interaction coefficients in the free energy potential are required to prevent unwanted phase-fields from contributing at interfaces. Depending on the system properties, it can be cumbersome to find appropriate values for these coefficients, as they are not related to a physical quantity. From a mathematical point of view, the evolution equations obtained in the two approaches, have different solutions. However, both phase-field approaches are suitable to study the statistics and mean field characteristics of grain growth in bulk materials, even if they do not result in identical dynamics for vanishing grains.

Recently, Eiken and Böttger[100] extended the Micress multiphase-field model, based on the approach of Steinbach et al.,[19,46,68] with a new solver which considers volumetric expansion. The phases were considered to have individual molar volumes which are functions of composition and temperature, which is in contrast with previous phase-field models. They investigated the solidification of multicomponent ductile cast iron (Fe-C-Si-Mn-Mg) on the microstructure scale. The consideration of volumetric expansion was found to be essential to correctly predict volume phase fractions as well as multicomponent segregation.

7. Phase-field models for extractive metallurgy

7.1. Phase-field modelling of redox reactions

Redox reactions occur quite frequently in extractive metallurgy, e.g., in electrometallurgy. However, most of the times, an electrode is not always explicitly present in the system. For example, the reaction of iron oxide dissolved in liquid slag with solid carbon or carbon from a metal bath is used in iron making processes. Modern electric arc furnaces employ the same reaction to induce slag foaming, thereby increasing efficiency of the furnace.[101,102] With a different purpose, iron oxide is reduced by injected carbon in the 'slag cleaning' stage of copper making processes. This reduces the present magnetite in the slag and thus lowers the slag viscosity, moreover, physical entrapment of copper matte in the slag is reduced.[103] Few existing phase-field models include the aforementioned redox reactions, which can take place at the interface between an electrolyte and a cathode or the interface between a metal and an oxide. The phase-field formulation of the electrochemical process is not straightforward because a model of the electric field has not been established for this method. Thus, a small amount of phase-field models considering electrochemical reactions are presented in literature. Moreover, they are usually not coupled to realistic systems. Different systems concerning redox reactions were already described with phase-field models, which are described in the following paragraphs.

7.1.1. Redox reactions on double-layer scale

Guyer et al.[104,105] developed a diffuse interface model for such a system. With a set of simple assumptions, the model captures the charge separation associated with the equilibrium double layer at the electrochemical interface for both electrodeposition and electrodissolution. The presence of charged species leads to rich interactions between concentration, electrostatic potential and phase stability. Poisson's equation (36) was solved for the electrostatic potentials arising from the charge density of the components.

$$\nabla\cdot[\varepsilon(\xi)\nabla\phi]+\rho=0 \tag{36}$$

With $\varepsilon(\xi)$ the dielectric constant, which is a function of the phase-field ξ, ϕ the potential and ρ the charge density. However, it is complicated to solve Poisson's equation for the electrostatic potential from the component itself since it is numerically challenging to solve this equation coupled with a time-dependent partial differential equation, resulting in a small time scale and meshing in space, as illustrated by the resulting interface profile during electrodeposition in Figure 7. Thus, it has only been solved in one dimension. The interface between the phases is a very localized change of the phase variable and is described well by the model. The need to resolve the charge distribution in close proximity of the interface, however, requires discretization of the electrochemical double layer and thus also limits the size of the domain and the time span that could be modelled. This model indicates that the phase-field model is suitable to model redox reactions but it considers an idealized system with only two phases (namely an electrode-electrolyte system). This is a nice model for investigating the scale of the interfacial double layer, but it is computationally too intensive to study the morphological changes resulting from redox reactions.

7.1.2. Redox reactions on a larger scale

Before Guyer et al.[104,105] developed their model, Dussault and Powell[106] described a diffuse interface model for a two component liquid–liquid, isothermal system undergoing transport limited electrochemical reactions, by assuming charge neutrality everywhere, resulting in the assumption of

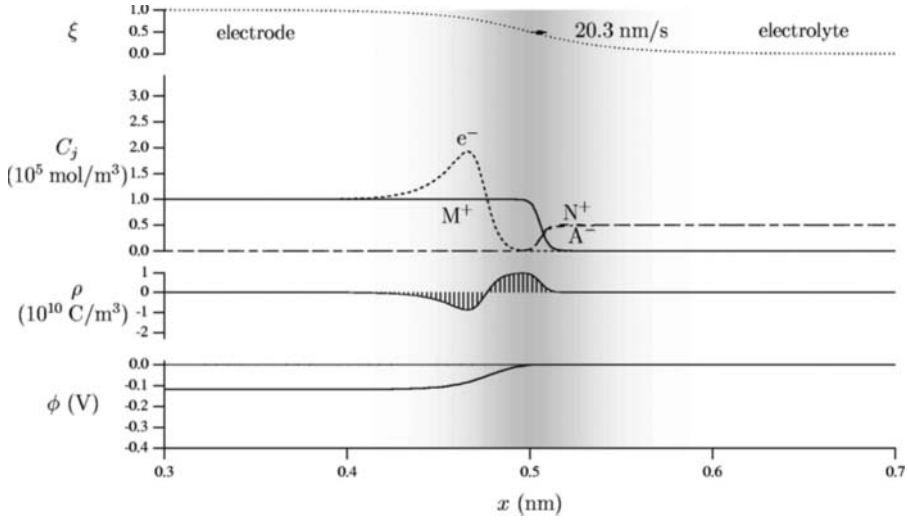

Figure 7. Interface profiles for steady state electrodeposition with $i = -10^2$ A/m^2. The concentration profiles for N^+ and A^- are almost coincident on this scale. $g(\xi)$ is mapped onto the background in gray to indicate the location of the phase-field interface. (© American Physical Society (Physical Review E). Reprinted with permission from Guyer et al.[105] Permission to reuse must be obtained from the rightsholder.)

very fast charge redistribution with respect to the relaxation of diffusion fields. Hereby avoiding to resolve the double layer and the resulting fine discretization.[107] First, very general forms of the governing equations were derived after which different scales were derived, which in turn were used to simplify the governing equations. For example, the conservation of charge equation involved only voltage with a spatial derivative after the simplification, without the originally present concentration or velocity. The electrical potential is only mentioned in the molar flux in a migration term, but the expression for the total free energy of the system itself does not contain the electrical potential. Thus their approach neglects the effects of charge at the interfacial double layer, resulting in the modelling of larger domains and time spans than Guyer et al.[104,105] but without the examination of the physics of the electrocapillary interface. In one of their simulations to resemble the Electric-Field-Enhanced Smelting and Refining (EFESR) process, an isolated Fe droplet was added to the slag layer (FeO). As shown in Figure 8, under an electric field, an isolated Fe droplet migrates through the slag. Comparing the result to the zero-voltage result, the drop and the interfaces migrate toward the anode. Also, due to the relatively high voltage gradients near the droplet, a streamer is formed on the cathode.

Assadi[108] used a phase-field model to investigate the electro-deoxidation of a solid oxide in a molten salt. That is, the direct electrochemical reduction of solid oxides in molten salts, during which the oxygen is removed from the solid oxide. The model takes into account oxygen diffusion, electric current, concentration dependence of electrical conductivity and interfacial electrochemical reactions in simple model systems. This model used the continuity of current density as the governing equation for electrical potential, except at the cathode-electrolyte interface. Its diffuse interface was between the metal and oxide in the cathode, and it assumed a sharp interface between the cathode and molten salt, with ohmic resistance at that sharp interface. The use of the sharp interface prevents its use to describe plating from the electrolyte, so this model is limited in application to electro-deoxidation; the assumption of ohmic resistance at the interface also limits it to small overpotential there.[109] The resulting simulations illustrate general features, such as a changing electric-potential drop at the cathode interface. The first results for a one-dimensional system show a transition from diffusion-controlled kinetics to kinetics controlled by electric conduction with decreasing oxide/metal conductivity ratio. For the two-dimensional system, nevertheless, the overall kinetics of electro-deoxidation is

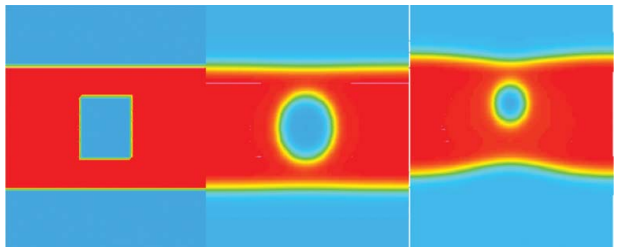

Figure 8. Phase-field model of droplet migration in the Fe-FeO system, setting the voltage to one at the upper boundary and zero at the lower boundary, with insulating conditions on the sides, makes the bottom Fe layer the cathode and the top the anode. Left: initial condition; Middle: zero-field result; Right: field concentration leading to drop migration. Colour represents oxide ion concentration, with the centre slag layer at its maximum and the outer metal layers at zero. (© Dussault and Powell. Reprinted with permission from Dussault & Powell.[106] Permission to reuse must be obtained from the rightsholder.)

predominantly controlled by the diffusion of oxygen in cathode.

Another phase-field model, developed by Pongsaksawad et al.,[109] improved the formulation of Dussault and Powell[106] by taking the electrostatic contribution in the free energy term into account, similar as presented by Guyer et al.[104,105] The binary model describes the electrochemical interface dynamics and studies the changes in cathode shape and topology. In this model, the interfacial double layer is negligible. Transport-limited electrolysis and rapid charge redistribution are assumed. Under this first condition, the mass-transfer resistance is much greater than the charge-transfer resistance. This means that cations recombine with electrons as soon as the ions reach the cathode interface. This transport-limited condition is valid at high temperatures (e.g., in metal smelting processes). Low-temperature processes, in contrast, are limited by charge transfer, which causes cations to accumulate in front of the cathode, resulting in a voltage drop across the interface, which is not captured by this model.

The model of Pongsaksawad et al.[109] describes all-solid and all-liquid binary and ternary systems, though mixed solid–liquid systems (e.g., solid electrode and liquid electrolyte) are not yet covered by this model. The motivating applications are the electric-field-enhanced smelting and refining process (EFESR) in which iron is reduced from liquid slag containing iron oxide, and magnesiothermic reduction of titanium dichloride. An illustration of the former is shown in Figure 9.

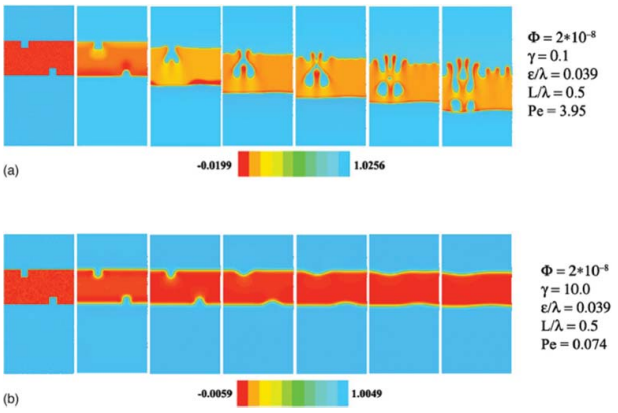

Figure 9. Interface dynamics without convection: (a) cathode shape evolution under high electric field on a 150 × 300 grid (the perturbed cathode interface is unstable) and (b) cathode shape evolution under high surface tension on an 80 × 160 grid (the perturbed cathode interface is stable). The left contour represents the initial condition with a three-layer structure, metal/electrolyte/metal. The cathode interface evolves with time as shown in the figures on the right. The scales on the bottom of each figure indicate the average maximum and minimum compositions throughout each simulation domain. (© Electrochemical Society (Journal of the Electrochemical Society). Reprinted with permission from Pongsaksawad et al.[109] Permission to reuse must be obtained from the rightsholder.)

Here a simplified three-layer structure of the binary system (Fe–FeO–Fe) is used as an initial condition. The voltage at the upper boundary is set to 0 (cathode) and that at the lower layer is set to 1 (anode). The interface instability due to change in electrical potential and surface energy is investigated first for the solid Fe–FeO system. One small box perturbation is introduced to each electrode interface. The perturbation on the anode disappears because it is preferentially oxidized and dissolved due to the concentration of the electric field there. At a low surface energy shown in Figure 9a, a large electrical potential results in the formation of dendrites at the cathode, which may short-circuit the system or break into droplets, as observed in experiments. At a larger surface energy shown in Figure 9b, the perturbation on the cathode is flattened. They also investigated the influence of viscosity on the electrode stability after perturbations and even performed 3D simulations. This phase-field model can ultimately result in a better understanding of the surface-stability of electrodes.

7.1.3. Electronically mediated reaction

The binary model of Pongsaksawad et al.[109] was extended to a ternary system. This model can capture electronically mediated reactions (EMR), such as metallothermic reduction. They simulated for example the reaction (without any voltage applied on the system) between titanium dichloride and magnesium to produce titanium and magnesium chloride. One- and two-dimensional ternary simulations show qualitatively correct interface motion and electrical potential behavior. However, this model assumes regular solutions with miscibility gaps, thus, the free energy includes logarithmic functions, such that values of zero and unity of phase variables are not allowed. Moreover, a chemical driving force for the redox reaction is introduced in the homogeneous free energy expression. But the argumentation behind the definition of this term is not clear, the use of this term is only applicable for the abovementioned system and the system is still idealized, i.e., it considers regular solutions. Further modification of this model is necessary to include multiphase systems, as at the moment it describes only all-liquid or all-solid systems. Figure 10 illustrates the results for a simulation where Mg and Ti are in contact, which allows the electrons from the $Mg/MgCl_2$ interface to be conducted through this metal phase to the $TiCl_2/Ti$ interface. The voltage is high where the positive charge is produced at the $TiCl_2/Ti$ interface and low where the electrons are produced at the $Mg/MgCl_2$ interface.

This observation clearly illustrates that this is an electronically mediated reaction (EMR), even though a high-temperature electrochemical reaction is a mass-transport limited process. Nonetheless, the electron transport between metals also has a significant effect on the product

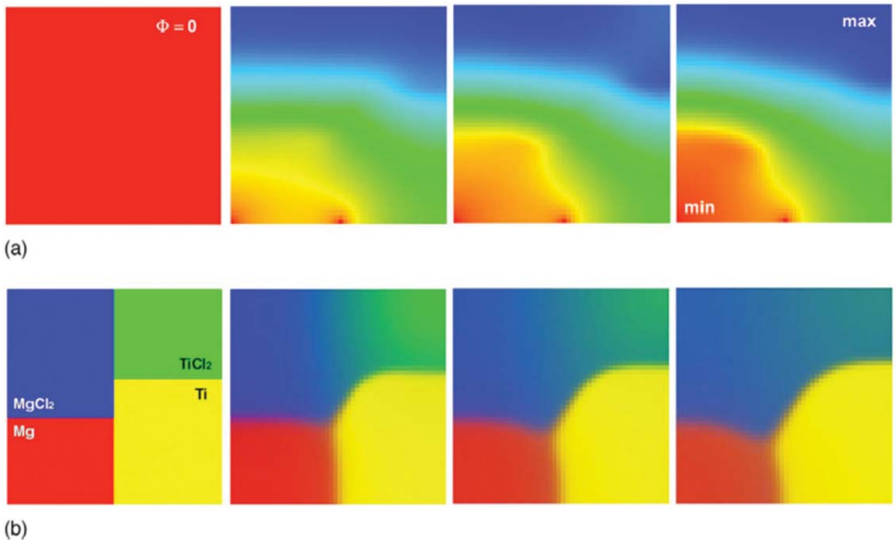

Figure 10. Closed-circuit simulation with Ti and Mg phases in contact. In the electrical potential contour plot, red indicates low and blue indicates high value of electrical potential, as labelled by min and max on the figure. The Mg, $MgCl_2$, $TiCl_2$, and Ti phases are coloured red, blue, green, and yellow, respectively, as also shown by labels. Ti formation is by chemical reduction at the Ti–Mg–chlorides triple point and by EMR between the Ti–$TiCl_2$ and Mg–$MgCl_2$ interfaces. The resolution is 50 × 50. (a) Electrical potential field. (b) Phase-field. (© Electrochemical Society (Journal of the Electrochemical Society). Reprinted with permission from Pongsaksawad et al.[109] Permission to reuse must be obtained from the rightsholder.)

morphology as explained by Okabe and Waseda.[110] This simulation illustrates that titanium can be formed even when the reactants ($TiCl_2$ and Mg) are not in physical contact as long as there is an electron conducting medium to transfer electrons (the metal phases).[109] A further demonstration of the EMR through the product Ti phase is illustrated by Figure 11, where Mg and $TiCl_2$ are set up to be in direct contact. The Ti phase then forms at this interface and in contact with the Mg, after which it serves as an electronically conducting path for the EMR.

Another test run was also done on a simple configuration of a three-layer structure (top: $TiCl_2$ – middle: Ti and $MgCl_2$ – bottom: Mg). First, titanium formation occurs by EMR due to movement of electrons from Mg-$MgCl_2$ interface through titanium to Ti-$TiCl_2$ interface. Later, diffusion of $TiCl_2$ reaches the magnesium layer and titanium nuclei form on the magnesium/electrolyte layer. These nuclei continue to grow. Finally, the small particles coarsen. These simulations suggest that magnesiothermic reduction is delayed when the direct contact between the reactants is blocked. However, since $TiCl_2$ can diffuse into the blocking layer, titanium particles still form spontaneously. All of these observations can be used to understand the basic phenomena that occur during the production process of Ti and to help design the experimental study.[111]

7.1.4. Deposition on electrode

Shibuta et al.[112] provide a model similar to the model of Pongsaksawad et al.,[109] but use an order parameter field with thin-interface limit parameters, which describe the motion of the interface quantitatively. The model is based on the description by Kim et al.[65] and can capture both deposition and dissolution processes during electrochemical processes. However, a dilute-solution approximation and an ideal-solution approximation are adopted to define the free-energy densities of the electrode and the electrolyte phase, respectively. Using this model, an electrodeposition process of copper deposits from copper-sulfate solution was studied. The dependence of the growth velocity of the electrode on the applied voltage was examined in a one-dimensional system. Then, the growth process of dendritic deposits of Cu was calculated in a two-dimensional (2-D) system. The dependence of morphology on the applied voltage and the electrolyte concentration was examined. Thin and dense branches were observed at a low applied voltage. The shape of the branches became more complicated as the composition ratio was lowered.

In the previous model,[112] the electrical current was considered in terms of the electric potential gradient in the equation of charge conservation. In that equation, the chemical potential gradient was neglected assuming electromigration to be the dominant factor determining the electrical current. This phase-field model processes can give an indication on the influence of important process parameters on the morphology of the produced electrodeposit, hereby avoiding short circuiting due to dendrite formation. The remaining problem in the phase-field model of the electrochemical process is how to treat the electrode reaction across the interface since the concept of a redox reaction at the interface was ignored in the previous model. More information

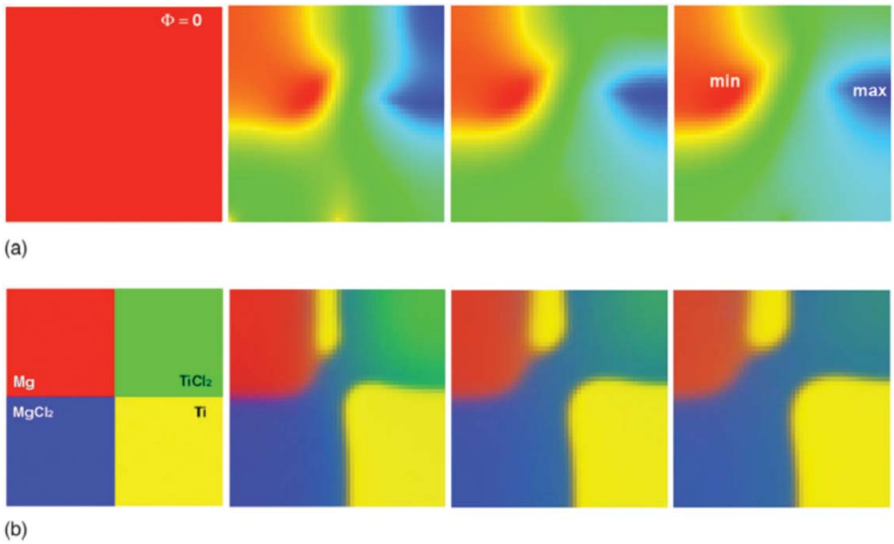

Figure 11. 2D model with Mg/$TiCl_2$ in contact. Titanium is first formed by a chemical reaction at the Mg/$TiCl_2$ interface. More titanium plating then proceeds by EMR as indicated by the change in voltage across that titanium phase. The resolution is 50 × 50. (a) Voltage field. (b) Phase-field. (© Electrochemical Society (Journal of the Electrochemical Society). Reprinted with permission from Pongsaksawad et al. [109] Permission to reuse must be obtained from the rightsholder.)

regarding phase-field modelling of electrodeposition can be found in Ref.[107]

7.1.5. Nonlinearity

The abovementioned phase-field models are limited to the case where the interface growth velocity is much smaller than the maximum velocity of the phase-field propagation and the linear thermodynamics where the driving free energies are much smaller than *RT*. This is because the models discussed up till now are based on linear thermodynamics. Okajima et al.[113] extended the previous model[112] by taking Butler-Volmer kinetics at the electrode/electrolyte interface into account. This was done by introducing a certain asymmetry, which is characteristic for redox reactions, to the diffusivity, with an exponential factor of the asymmetry coefficient. Using this model, the kinetics and morphology of the electrode/electrolyte interface during an electrode reaction have been investigated. The numerical results satisfied the Nernst relationship and confirmed the relation between the growth velocity of the interface and the overpotential. The tip radius is, in turn, proportional to the inverse of the square root of the growth velocity, which agrees with the dendrite growth theory for solidification. Even though the model includes several assumptions (ideal solution and ideal diluted solutions for the electrolyte and electrode, respectively), it shows that phase-field simulations can be helpful to clarify complicated electrochemical reactions.

In a similar way, Ma et al.[114] used an Arrhenius relationship in the expression for the coefficient of the Cahn-Hilliard equation, which describes the evolution of the oxidation state of the material. However, in both these models, the diffusional mobility might have an exponential dependence on the overpotential, but the rate of electroplating is still linearly proportional to the thermodynamic driving force. Later, Liang et al.[115] developed a more intricate nonlinear phase-field model for electrode-electrolyte interface evolution driven by the overpotential. They wanted to describe the temporal and spatial evolution of the phase-field variable by the difference of two exponentials of the driving force, motivated by classical rate theory of chemical reaction kinetics. However, a simplified form of the nonlinear equation was required and thus the interface migration velocity was assumed to be linearly proportional to the interfacial energy reduction, but nonlinearly with respect to the overpotential.

7.1.6. Incorporation of chemical reaction kinetics

Based on the work of Sekerka and Bi,[116] Gathright et al.[117] presented a phase-field model for an electrochemical system with chemically active species. They explicitly incorporate a term including the rate of the chemical reaction(s) under consideration. One big disadvantage for such a model is the fact that knowledge is required about which reactions take place in the system and care must be taken that none are forgotten, to be able to model a realistic system. The latter is easy for a binary system, but becomes less self-evident for multicomponent systems. Later, Hong et al.[118] used a similar model to investigate the ionic/electronic transport across the cathode/electrolyte interface in solid oxide fuel cells.

Bazant[119] developed a phase-field theory of electrochemical kinetics by combining charge-transfer theory with concepts from statistical physics and nonequilibrium thermodynamics. It resulted in a single equation that generalizes the Cahn-Hilliard and Allen-Cahn equations for reaction-diffusion phenomena and it is called Cahn-Hiliard reaction (CHR) model. For charged species, the theory generalizes the Poisson-Nernst-Planck equations of ion transport, the Butler-Volmer equation of electrochemical kinetics and the Marcus theory of charge transfer for concentrated electrolytes and ionic solids. This equation was used by Cogswell and Bazant[120] to study the physics of nucleation in solid single-crystal nanoparticles, more explicitly: the model is used to simulate phase separation in realistic nanoparticle geometries for Li_xFePO_4, which is used as a cathode material in Li-ion batteries. They showed that the nucleation in single-crystal nanoparticles is size-dependent, due to surface adsorption which leads to coherency strain. Thus, the nucleation barrier decreases with the area-to-volume ratio. The model was extended to three phases and was used to simulate lithium intercalation in a porous iron phosphate cathode and was also used to investigate the changing phase transformations between the three stable phases in a porous graphite anode by Ferguson and Bazant.[121] For the latter, Figure 12 illustrates a comparison between experimental observations and the simulation results. For both processes, the phases present were assumed to be regular solutions. This phase-field model can give an indication on the influence of important process parameters on the intercalation of anodes in commercial batteries, or more fundamentally, can give a better understanding of the processes taking place in the system.

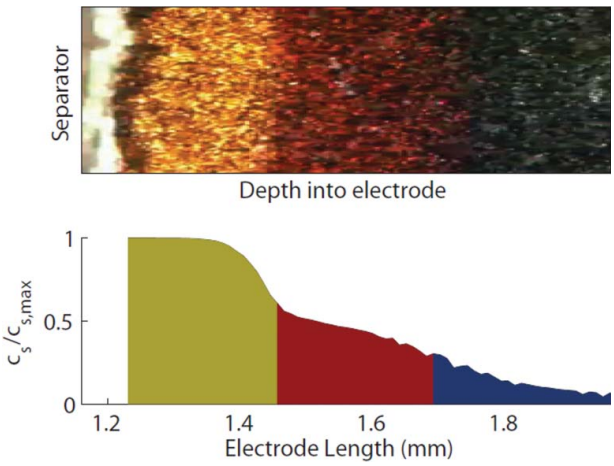

Figure 12. Graphite MPET simulations vs. experiment. Experimental image (above) and simulated colour profile (below) at the same moment in time, capturing the blue/red and red/gold interface positions and noise. (© Elsevier (Electrochemica Acta). Reprinted with permission from Ferguson & Bazant.[121] Permission to reuse must be obtained from the rightsholder.)

Heo et al.[122] also used the CHR model to simulate diffusional phase microstructural evolution at solid surfaces. Depending on the strength of the interaction between the solute and the interface, two different surface spinodal decomposition modes were predicted: the surface mode of coherent spinodal decomposition and the surface-directed spinodal decomposition mode. In the former, no explicit interaction between the solute atoms and the surface can be observed, whereas in the latter, the interaction induces surface segregation of the solute that acts as the dominant perturbation of the surface composition, over the natural thermal fluctuations, resulting in surface-initiated spinodal decomposition. Kappus and Horner[123] investigated spinodal decomposition in metal hydrides and alloys near a surface. They found that the surface spinodal decomposition happens faster than the bulk spinodal decomposition as long as the crystal is coherent. They developed a statistical theory containing thermal fluctuations and nonlinear effects and solutions were found in a mean field approximation. Tang and Karma[124] also showed that free surfaces influence spontaneous phase separation in elastically coherent solids with linear stability theory and numerical simulations. The faster kinetics of surface modes with respect to bulk modes can be found in the misfit stress relaxation near surfaces. This phenomenon was also observed by Bellemans et al.[125] in a system where the spinodal decomposition takes place in a liquid phase and was denoted 'localized spinodal decomposition'.

7.1.7. Metal oxidation and possible stress generation

Asle Zaeem and El Kadiri[126] elaborated on a multiphase-field model for nonselective oxidation of metals incorporating both the oxidation kinetics and stress generation by coupling the phase-field evolution equations to the mechanical equilibrium equations with the use of COMSOL.[127] The model predicts the oxygen composition depth and stress profile in the oxide layer and the metal-oxide interface and proved its usefulness by prediction of the observed evolution of oxide thickness and growth stresses for the oxidation of Zircaloy-4 at 900 °C, which is actually a commercially available alloy used in nuclear technology. They concluded that the oxidation generates stresses, which in turn slows down the oxidation kinetics.

Apel et al.[128] and Berger et al.[129] used the MICRESS[130] software to simulate the microstructure evolution in Ag-Cu brazing fillers for conditions close to reactive air brazing (a method commonly used to join metals to ceramics). The simulations were then used to calculate the volume expansion due to phase transformations (and the resulting eigenstrains) and DSC curves, allowing comparison to experimental observations. However, due to the lack of thermodynamic databases for the brazing filler material in

combination with data for the substrate materials, any reaction between brazing filler and base materials were neglected in the simulations. One of the obtained simulation results for an Ag-Cu brazing filler is shown in Figure 13.

Similarly, Ta et al.[131] used MICRESS[130] to investigate the effect of a temperature gradient on the microstructure evolution in various Ni-Al-Cr bond coat/substrate systems, which are used for airplane turbines. As a complete database of the system was present in this case, the phase-field model was coupled to a CAPLHAD database, yielding quantitative results.

Recently, Sherman and Voorhees[132] employed the phase-field method to model an electrochemical interface between an oxide and a metal in contact with a gas, specifically for protective oxide phases such as Cr_2O_3 and Al_2O_3. The model includes a hybrid ideal solution and free electron gas description of the bulk thermodynamics and explicitly considers a defect structure. They showed that the protective oxide phases inhibit corrosion kinetically and not thermodynamically.

7.2 Phase-field modelling of wetting

Wetting at high and low temperatures is important in pyro- and electrometallurgical processes, respectively, both types of processes being essential during extractive metallurgy. In all these processes, (non-)wetting may play an important role to deteriorate or improve the phase separation between different phases, e.g., the attachment of the metal phase to certain solid particles within the liquid slag which hinders their sedimentation.[133–139] Wetting is generally subdivided in nonreactive and reactive wetting, which were both already modelled with the phase-field method.

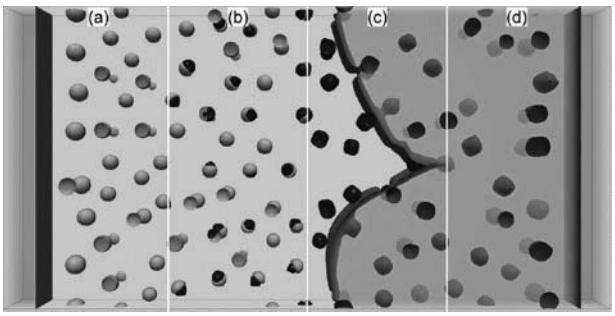

Figure 13. Simulated microstructure evolution during RAB, left to right: (a) 1238 K, demixed L_2 (a Cu-rich liquid phase) drops in L_1 (transparent, an Ag-rich liquid phase), (b) 1223 K, $L_2 \rightarrow$ CuO reaction, (c) 1183 K, $L_1 \rightarrow$ fcc reaction, (d) 1168 K, solidified fcc-Ag with embedded oxide particles (CuO).Microstructure evolution in a brazing joint, Ag8at%Cu. The simulation clearly indicates the general phase formation sequence according to the phase diagram: $L_1+L_2 \rightarrow L_1 + CuO \rightarrow CuO + fcc\text{-}Ag$. (© John Wiley and Sons (Advanced Engineering Materials). Reprinted with permission from Berger et al.[129] Permission to reuse must be obtained from the rightsholder.)

7.2.1. Nonreactive wetting

Wetting of a foreign wall by fluids has been studied extensively. Various methods have been applied to address these problems such as continuum models and atomistic simulations. Despite this inventory, recent studies addressing heterogeneous crystal nucleation rely almost exclusively on the classical spherical cap model, which assumes mathematically sharp interfaces.[140,141]

If the action of the solid on the density field is short ranged compared to the thickness of the diffuse interface, it can be accounted for by appropriate boundary conditions at the solid surface. Typically, a simple Dirichlet boundary condition is enforced on the solid surface.[142] From this boundary condition, a certain 'standard' contact angle can be derived, but this value has nothing to do with a 'true' contact angle at the solid surface. The latter is not defined in these phase-field models, since different iso-levels behave in qualitatively different ways as the solid surface is approached. The only level that hits the solid surface at the right angle is the one with the value of the Dirichlet boundary condition. Another option to introduce fluid-wall interactions is the use of a third phase-field with a very high viscosity to represent a solid wall.[143]

With regard to heterogeneous nucleation, the phase-field method has also been used to describe a system with an arbitrary contact angle. Here the wall-liquid and wall-solid interactions are characterized by the contact angle θ that is determined from the interfacial free energies by Young's equation: $\gamma_{WL} = \gamma_{WS} + \gamma_{SL}\cos(\theta)$, where subscripts W, S, and L refer to the wall, the solid, and the liquid, respectively. Both a single component system[140] and a binary alloy system[141] were already investigated. Numerical approaches to obtain a certain wetting behavior are designed to either ensure the desired contact angle or fixing the value of the phase-field at the wall or the normal component of the phase-field gradient.[140,141] The three different models are also illustrated in Figure 14 and can be summarized as:[140,141]

- Model A is a diffuse interface implementation of the classical spherical cap model with a contact angle that is independent of the driving force. This contact angle is ensured by a specific surface function. This model places the mathematical surface at which the boundary condition acts slightly beyond the boundary layer. Thus, the bulk liquid and solid phases in contact with the wall are connected through an unperturbed solid–liquid interface profile, and the derivation of the interface function for the desired contact angle is

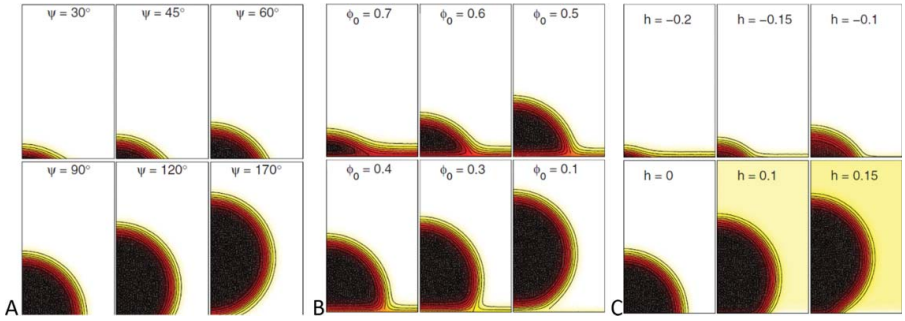

Figure 14. Structure of heterogeneous nuclei in model A for various contact angles; in model B for various phase-field values at the wall and in model C for various values of the gradient of the phase-field variable. There is a symmetry plane on the left edge of every simulation. The contour lines of the phase-field variable vary between 0.1 and 1.0 by increments of 0.1. (© American Physical Society (Physical Review B). Reprinted with permission from Warren et al.[141] Permission to reuse must be obtained from the rightsholder.)

straightforward. The total free energy of the system incorporates both a volumetric and a surface contribution.

- Model B is a nonclassical formulation assuming a fixed phase-field value at the interface, leading to certain surface (dis)ordering, a strongly supersaturation-dependent contact angle. In this model, only local states present in the solid–liquid interface can be realized at the wall. A shortcoming of this model is its implicit assumption that the wall enforces the formation of a specific layer of the solid–liquid interface. In this case, the free energy of the system only consists of a volumetric contribution.
- Model C is a nonclassical approach, which fixes the normal component of the phase-field gradient, leading to surface (dis)ordering, a supersaturation-dependent contact angle. This model has a less straightforward physical interpretation, but can prescribe local conditions that are not present at the solid–liquid interface.

Bellemans et al.[125] considered a hypothetical binary system O-M to investigate different wetting regimes of liquid metal droplets on solid particles within liquid slags. A nonconserved phase-field variable ϕ was combined with a conserved composition field x_M. It was assumed that the concentration of the solute in the precipitate was fixed and the solid particles were assumed to be present before droplet formation.

Especially noteworthy about the developed model was the expression for the solid–liquid interfacial energy (J/m^2) $\gamma_{S,L}$, as it consisted of a contribution following the approach of Allen and Cahn[31] and a second term originating from a combined variation of ϕ and x_M across the solid–liquid interface. This yields a nonzero gradient term for x_M. Because this contribution cannot be evaluated analytically, the following assumption was made: the composition dependence of the Gibbs energy across the interface is approximated by a spinodal function. This gives a dependence of the second term in the solid–liquid interfacial energy on x_S, the constant composition of the solid particle. This approximation was validated by the measurement of the contact angles in several simulations,[125] and the observed values agreed well with the predicted values.

The definition and characterization of the three regimes illustrated in Figure 15[125] from the simulations can help to classify and interpret experimental observations and measurements of the attachment of metal droplets to solid particles in liquid oxides. Comparison of experimental results for a PbO-FeO-CaO-SiO_2-Cu_2O-ZnO-Al_2O_3 system[133] with the simulations, indicated that this system corresponds to the low wettability case. Moreover, the influence of the morphology and fraction of the solid particles on the attachment behavior of the metallic droplets was evaluated.[144] The model was further extended[145] to also consider the movement of the solid phase with respect to the liquid phases. A clear influence on the wetting (i.e., the apparent contact angle of the metal on the solid) was observed. This could indicate that the previous classification of the experimental system as one with very low wettability is slightly different.

7.2.2. Reactive wetting

Reactive wetting also involves redox reactions, albeit without the presence of an electrode. Villanueva et al.[146–148] developed a phase-field model for this. Reactive wetting involves a chemical change and/or diffusion of chemical species. Thus, the motion of the contact line is controlled by diffusion of species and capillary effects. In these models, the substrate is allowed to dissolve and consequently

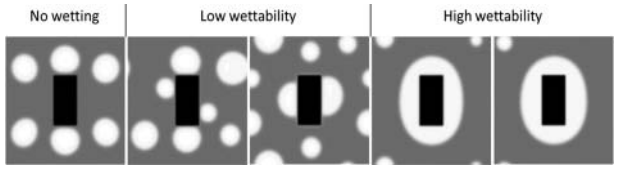

Figure 15. Different wetting regimes resulting from a variation in interfacial energies. Dark grey: the oxidic liquid (slag); white: the metallic liquid (alloy droplet); black: solid particle (nonreactive).

there is no guarantee that the system will relax toward the equilibrium contact angle given by the Young's equation.[143] There are two cases: a concentration change of the spreading liquid and the substrate or the formation of a new phase or phases between the liquid and the substrate. The first case was modelled by Villanueva et al.[146,147] Their model describes a ternary system of substitutional elements with three phases in a system with fluid motion, by introducing convective concentration and coupling to Navier–Stokes equations with surface tension forces.

$$\rho(\phi)\left(\frac{\partial u}{\partial t}+u\cdot\nabla u\right)=-\nabla\tilde{p}+\nabla\cdot\mu(\phi)\left(\nabla u+\nabla u^{T}\right)$$
$$-\sum_{i=L,S,V}\phi_i\nabla\left(\frac{\delta G}{\delta\phi_i}\right)-\sum_{i=L,S,V}x_i\nabla\left(\frac{\delta G}{\delta x_i}\right) \quad (37)$$

With ρ the density, u representing an incompressible flow, $\tilde{p}$ a nonclassical pressure, μ the viscosity and φ_i the phase-field variables. The solid substrate is modelled hydrodynamically with a very high viscosity. For simplicity, an ideal solution was assumed to describe the molar Gibbs free energy and the thermodynamic data were retrieved from simple and idealized phase diagrams. Two stages occurred in the wetting process: a convection-dominated stage where rapid spreading occurs and a diffusion-dominated stage where depression of the substrate–liquid interface and elevation of the contact line region were observed.

The first binary model of Villanueva et al.[146,147] considers droplets that do not exhibit inertial effects due to the small drop size, which is limited by the requirement of having a narrow interface (≈1 nm). Wheeler et al.,[149] in contrast, sacrificed the realistic interface width in an attempt to model a system that exhibits inertial effects. Due to the drop size restrictions, the extent of spreading during the inertial stage is limited and the characteristic inertial effects are suppressed by viscous forces. They investigated a three-phase binary alloy in a parameter regime where the inertial effects were initially dominant and the transition from inertial to viscous or diffusive spreading is also characterized well. At late times, after inertial effects have ceased, the local interface equilibration mechanism is controlling the spreading.

The first binary model of Villanueva et al.[146,147] was expanded to a ternary system with four phases to model reactive wetting with intermetallic formation,[148] also incorporating fluid flow, phase change and solute diffusion. Numerical simulations were performed using a mesh-adaptive finite element method, revealing the complex behavior of the reactive wetting process, an illustration is shown in Figure 16. Dynamic results showed that the intermetallic can either precede or follow the spreading liquid droplet, depending on the time and the choice of interface energy and kinetic coefficients.

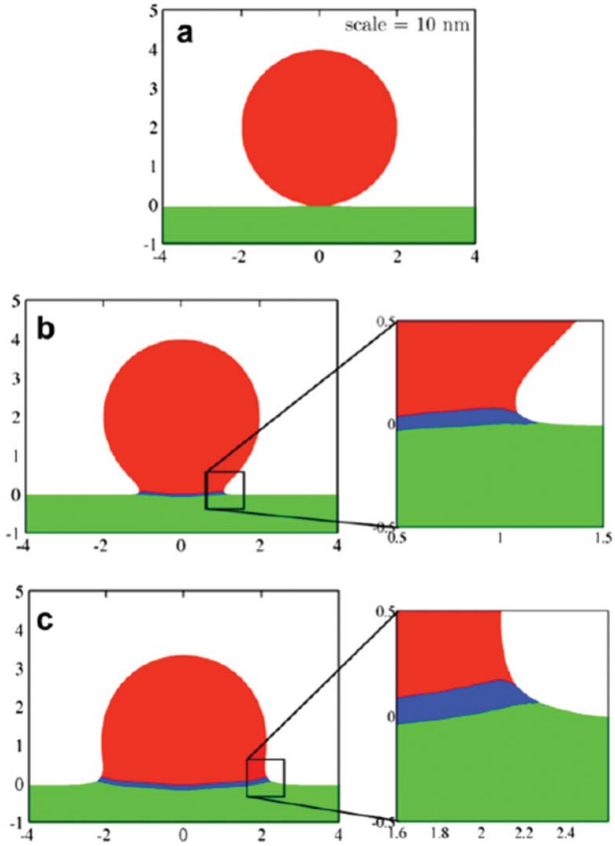

Figure 16. Simulation result of the maximum phase-field plot at $t/t_c = 0$, 1, 200 with the base set of parameters. (© Elsevier (Acta Materialia). Reprinted with permission from Villanueva et al.[148] Permission to reuse must be obtained from the rightsholder.)

However, the model still used thermodynamic data derived from a classical phase diagram, while assuming an ideal solution model for the Gibbs free energy of the liquid, solid, and vapor and a regular solution model for the Gibbs free energy of the intermetallic phase. Moreover, only small system sizes can be simulated with this model.

Later, Wang and Nestler[150] investigated the formation of an Al_2Au intermetallic phase at the interface between an Al-liquid droplet on top of an Au solid substrate with 3D simulations. They also present a new concept that lateral spreading of the intermetallic phase is due to wetting, which differs from the idea of grain boundary diffusion.

By placing an Al-liquid droplet on an Au-solid substrate, the amount of Au in the liquid tends to approach the equilibrium mole fraction. This is achieved by diffusion of Au into the Al-liquid. Thereafter, Al and Au combines with a ratio of 2, forming the intermetallic phase Al_2Au. Due to the surface energy relation: $\gamma_{SL} > \gamma_{SI} + \gamma_{LI}$, the triple point of solid–liquid–intermetallic phase is not stable, resulting in the growth of the

intermetallic phase in the horizontal direction. This relation was also proposed by Villanueva et al.[148] for the intermetallic Sn–0.7Cu on a Cu substrate. During the spreading of the intermetallic phase, the Au atoms constantly diffuse into the Al-liquid, which provides the source for the later growth of the intermetallic phase in the vertical direction. When the two triple points SIV and LIV are established, i.e., when the solid–liquid interface is completely covered by the intermetallic phase, the spreading of the intermetallic phase in the horizontal direction stops. The intermetallic phase then grows in the vertical direction, increasing its thickness. At this stage, the liquid is no longer in contact with the solid. Since the diffusivity of Au in liquid Al is greater than the one in solid Au, the intermetallic phase grows into the liquid droplet. This is also illustrated in Figure 17.

7.3. Phase-field modelling of solidification in oxidic systems

The abovementioned models describe idealized systems and are only coupled to thermodynamic databases in a limited manner, as they use assumed ideal solutions or diluted solutions to describe the Gibbs free energies of the different phases. A slag phase is a mixture of metal oxides and silicate melts typically consist of a network of Si-ions, introducing a certain ordering in the phase. Thus, the phase has a structural complexity that cannot be described by ideal or regular solutions. To describe the Gibbs energy of a slag phase, the modified quasi-chemical model was introduced by Pelton et al.[151–154] and describes the Gibbs energy as a function of the pair fractions, amongst others. The description is quite intricate for more than two components and thus it becomes appropriate to establish a coupling with a thermodynamic database (which essentially calculates Gibbs energies using the modified quasi-chemical model).

Heulens[155] modelled the crystallization of oxide melts. He implemented a multicomponent, multiphase system, and coupled the model with a thermodynamic database for oxides (FTOxid from Factsage/Chemapp) to obtain the bulk thermodynamic properties of the liquid slag as a function of composition. The stoichiometric solid phases were modelled with a paraboloid Gibbs energy with specific constraints to ensure correct phase equilibria and minimal solubility in the stoichiometric phase and the interfacial mobility and interfacial energy were modelled with anisotropy, as both faceted and dendritic growth morphologies are important for crystallization in oxide systems. The model was able to describe both crystallization and dissolution of the stoichiometric phase. The influence of the surface energy on the crystallization of wollastonite ($CaSiO_3$) is illustrated in Figure 18. The crystallization of oxide melts is an important phenomenon in many application domains, such as geology, pyrometallurgy, glass ceramics and advanced ceramic materials.

He also treated the redox dependent behavior of multivalent cations when an oxygen-containing atmosphere is present above an iron-containing melt.[156] If such an iron-bearing silicate melt is not in thermodynamic equilibrium with its oxygen-containing atmosphere, the melt is subjected to a redox reaction. In this model, the diffusion is assumed to be much slower than the redox reaction kinetics, and the redox ratio of FeO/Fe_2O_3 is thus locally in equilibrium with the oxygen activity in the melt. He simulated the crystallization of Fe_3O_4 in FeO_x-SiO_2 melts under oxidizing conditions. The oxidizing conditions were present on the upper boundary of the system with a condition to ensure conservation of Fe while the FeO/Fe_2O_3 ratio is in equilibrium with the oxygen fugacity of the atmosphere. Two-dimensional simulations were performed with different nucleation densities of Fe_3O_4 and varying oxygen fugacity in the atmosphere. He concluded that, for the considered nucleation densities, the crystallization of the melt has a larger effect on the oxidation state than the oxygen fugacity of the atmosphere. This is illustrated in Figure 19.

Liu et al.[157] also used this model to simulate the isothermal crystallization of wollastonite in the CaO-Al_2O_3-SiO_2 system. The effects of composition and temperature on the crystallization behavior were studied. The simulations show that for the considered cases, the wollastonite morphology

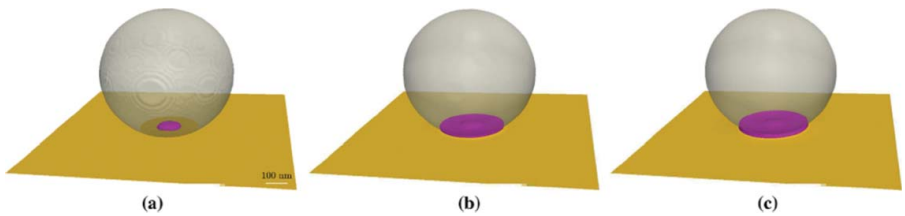

Figure 17. Time evolution of the intermetallic phase Al_2Au from a phase-field simulation: (a) Earlier stage of the intermetallic phase Al_2Au inside the Al-droplet, (b) spreading of the intermetallic phase in the horizontal direction, (c) growth of the intermetallic phase in the vertical direction. (© Elsevier (Acta Materialia). Reprinted with permission from Wang & Nestler.[150] Permission to reuse must be obtained from the rightsholder.)

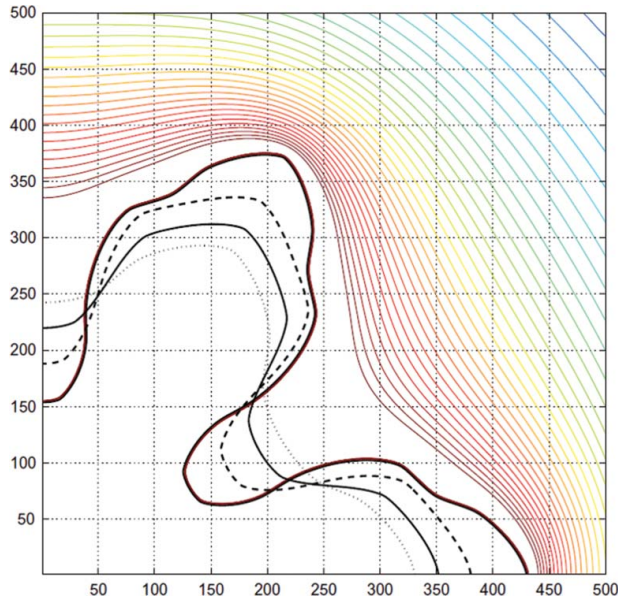

Figure 18. Simulation results of 2-D crystallization of wollastonite in a $CaO–Al_2O_3–SiO_2$ melt with four different surface energies, 0.3 (outer solid), 0.4 (dashed), 0.5 (solid), and 0.6 J/m^2 (dotted), and sixfold symmetry as observed in experiments. As the interfacial energy increases, the tip radius increases while the dendrite tip velocity decreases. For the simulation with $r = 0.3$, the diffusion field of Al_2O_3 is plotted as well. The system size is 12.5 × 12.5 μm, and the total simulation time for all four cases was 0.2226 s. Only the left lower quarter of the simulation domain is plotted to increase the readability. (© Elsevier (Acta Materialia). Reprinted with permission from Heulens et al.[155] Permission to reuse must be obtained from the rightsholder.)

is mainly determined by anisotropy in the interface energy and hardly affected by anisotropy in the interface kinetics. Some simulated shapes of isothermally crystallyzed wollastonite at different undercoolings are compared with the experimental observations in Figure 20.

In agreement with the observations from in-situ experiments,[158,159] the simulations show a transition from planar (a) to dendritic (b and c) growth with decreasing temperature and the dendritic structure becomes finer (c) when the temperature is decreased in further. Even though the experiments and simulations correspond well qualitatively, the temperature at which the transition occurs deviates from the experiment. A possible reason for these deviations between experiments and simulations is the intrinsic error in the experimentally determined temperatures. The transition from a flat to dendritic growth with decreasing temperature can be primarily explained by an instability of the planar interface due to the larger driving force for crystallization at higher undercoolings.

Later, Liu et al.[160] also used this model to investigate the dissolution of Al_2O_3 in a $CaO-Al_2O_3-SiO_2$ slag. The simulation results fit well to the analytical solution for dissolution in a one dimensional system and the dissolution rate of a circular Al_2O_3 particle. The simulations also agree well with experimental data.[161] Furthermore, the simulation results demonstrate that (1) the dissolution rate of Al_2O_3 increases with temperature, (2) the dissolution rate increases with increasing CaO content and with decreasing Al_2O_3 content for a fixed CaO/SiO_2 ratio.

8. Conclusions and future perspectives

This review paper introduces the phase-field method and gives an overview of its possibilities in extractive metallurgy. The phase-field method is a versatile and powerful technique for simulating microstructural evolution. It was already applied to solidification, precipitate growth and coarsening, martensitic transformations and grain growth, solid-state transformations, dislocation dynamics, crack propagation and nucleation.

In the phase-field method, the microstructure of a system is represented by a set of conserved and nonconserved phase-field variables that are continuous functions of space and time. Within the bulk of a domain, the phase-field variables have nearly constant values, and at the interface the variables vary

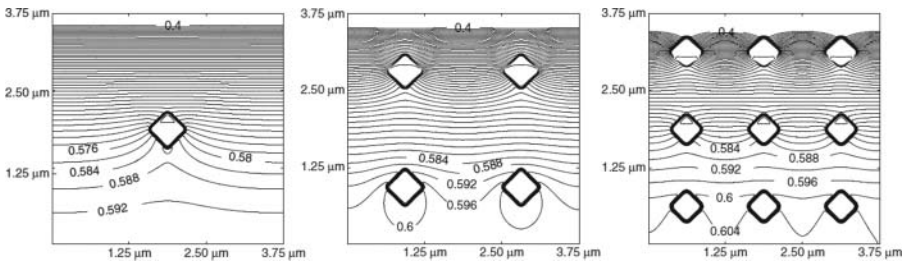

Figure 19. Contour plots of the mole fraction of FeO, showing the effect of the number of nucleation sites. From left to right, the number of crystal nuclei is 1, 4 and 9 and corresponds to a nucleation density of 7.1 × 10^6 cm^{-2}, 2.8 × 10^7 cm^{-2}, and 6.4 × 10^7 cm^{-2}, respectively. All three contour plots are scaled between $x_{FeO} = 0.40$ and $x_{FeO} = 0.62$ with a step of 0.004. The oxygen fugacity of the atmosphere was $f_{O2} = 1.5 \times 10^{-3}$ while the melt has initially an equilibrium oxygen activity of $a_{O2} = 2.4 \times 10^{-5}$. (© Elsevier (Chemical Geology). Reprinted with permission from Heulens et al.[156] Permission to reuse must be obtained from the rightsholder.)

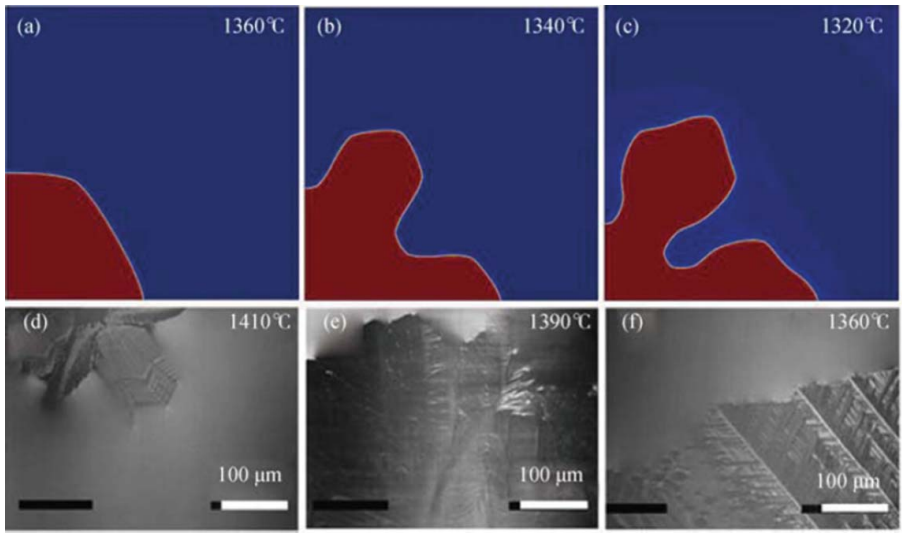

Figure 20. Simulated and experimental morphologies of wollastonite for different undercoolings for slag A (initial composition 42wt%CaO – 48wt%SiO_2 – 10wt%Al_2O_3): (a) $\Delta = 65°C$; (b) $\Delta = 8°C$; (c) $\Delta = 105°C$ after a simulation time of 1 s and (d) $\Delta = 15$ °C; (e) $\Delta = 35$ °C; (f) $\Delta = 65$ °C observed in the experiments. (© Editorial Board of Inorganic Materials (Journal of Inorganic Materials). Reprinted with permission from Liu et al.[157] Permission to reuse must be obtained from the rightsholder.)

continuously over a narrow region between their values in the neighboring domains. With the use of this diffuse-interface approach, no boundary conditions are required for the moving interface. With this approach, the models are able to predict complex morphological evolutions.

The free energy of the system is expressed as a functional of the phase-field variables and their spatial gradients. The temporal evolution of the phase-field variables is described by a set of kinetic equations which are solved numerically. The numerical solution and implementation of these evolution equations is relatively simple and straightforward, as there is no need to explicitly keep track of the interfaces. This review paper also lists descriptions of various phase-field models used to describe processes in extractive metallurgy.

Although the examples illustrate that the phase-field method has been successfully applied to numerous applications, it is still a challenge to apply the phase-field method to multicomponent systems and for realistic conditions. So far, most models consider idealized and simplified systems and only few simulations were performed in real ternary and quaternary systems, even less for oxide systems or systems containing both metals and oxides. Therefore, further optimization of coupling to thermodynamic databases and mobility databases is required. However, the latter are rare and mostly contain data on very specific simple systems. Other input data, such as surface tensions and interfacial energies, are also difficult to find in literature, as the experimental determination of them is extremely intricate. In this regard, further development of first principles methods will deliver more reliable results for more complex structures (for example, the interface energy, mobilities, etc.), which can then be used as input for the phase-field method. The microstructures resulting from the phase-field simulations can then also be used for more macroscopically oriented models, hereby stimulating multiscale modelling. For more realistic simulations, the incorporation of the reaction kinetics of the different phases could be a next possible step. At the moment, a lot of simulations assume diffusion-controlled growth, which is not always the case in reality. More efficient numerical implementations can also yield the possibility of 3 dimensional simulations, which are typically much more computationally extensive.

Acknowledgment

I. Bellemans holds a Ph. D. fellowship of the Research Foundation – Flanders (FWO).

ORCID

Inge Bellemans http://orcid.org/0000-0002-6171-8695

References

1. A. Karma and W.-J. Rappel, Quantitative phase-field modeling of dendritic growth in two and three dimensions. *Phys. Rev. E* **57**, 4323–4349 (1998).
2. W. J. Boettinger, J. A. Warren, C. Beckermann, and A. Karma, Phase-field simulation of solidification. *Annu. Rev. Mater. Res.* **32**, 163–194 (2002).
3. J. Heulens, Isothermal crystallization of metallurgical slags: phase field simulations combined with in situ

experiments (Isotherme kristallisatie van metallurgische slakken: faseveldsimulaties in combinatie met in situ experimenten). (PhD diss., KU Leuven, 2011). at <https://lirias.kuleuven.be/handle/123456789/318339>
4. L.-Q. Chen, Phase-field models for microstructure evolution. *Annu. Rev. Mater. Res.* **32**, 113–140 (2002).
5. Y. U. Wang, Computer modeling and simulation of solid-state sintering: A phase field approach. *Acta Mater.* **54**, 953–961 (2006).
6. L.-Q. Chen and W. Yang, Computer simulation of the domain dynamics of a quenched system with a large number of nonconserved order parameters: the grain-growth kinetics. *Phys. Rev. B* **50**, 15752–15756 (1994).
7. D. Rodney and Y. Le Bouar, Phase field methods and dislocations. *Acta Mater.* **51**, 17 (2003).
8. H. Henry and H. Levine, Dynamic instabilities of fracture under biaxial strain using a phase field model. *Phys. Rev. Lett.* **93**, 105504 (2004).
9. R. Spatschek, E. Brener, and A. Karma, Phase field modeling of crack propagation. *Philos. Mag.* **91**, 75–95 (2011).
10. D. N. Bhate, A. Kumar, and A. F. Bower, Diffuse interface model for electromigration and stress voiding. *J. Appl. Phys.* **87**, 1712–1721 (2000).
11. D. Raabe, Modeling and Simulation in Materials Science, in *Comput. Mater. Sci.* 111–118 (Wiley-VCH Verlag GmbH & Co. KGaA, 1998). at <http://onlinelibrary.wiley.com/doi/10.1002/3527601945.ch8/summary>
12. R. S. Qin and H. K. Bhadeshia, Phase field method. *Mater. Sci. Technol.* **26**, 803–811 (2010).
13. L.-Q. Chen and Y. Wang, The continuum field approach to modeling microstructural evolution. *JOM* **48**, 13–18 (1996).
14. N. Moelans, B. Blanpain, and P. Wollants, An introduction to phase-field modeling of microstructure evolution. *Calphad* **32**, 268–294 (2008).
15. M. Plapp, Remarks on some open problems in phase-field modelling of solidification. *Philos. Mag.* **91**, 25–44 (2011).
16. J.-O. Andersson and J. Ågren, Models for numerical treatment of multicomponent diffusion in simple phases. *J. Appl. Phys.* **72**, 1350–1355 (1992).
17. I. Steinbach, Phase-field models in materials science. *Model. Simul. Mater. Sci. Eng.* **17**, 073001 (2009).
18. A. M. Meirmanov, *The Stefan Problem*. Walter de Gruyter, Berlin, Germany (1992).
19. I. Steinbach et al., A phase field concept for multiphase systems. *Phys. Nonlinear Phenom.* **94**, 135–147 (1996).
20. H. Ravash, 3D phase-field simulations of sintering and coarsening in polycrystalline multi-phase materials. (PhD diss., KU Leuven, 2014).
21. J. A. Warren, R. Kobayashi, A. E. Lobkovsky, and W. Craig Carter, Extending phase field models of solidification to polycrystalline materials. *Acta Mater.* **51**, 6035–6058 (2003).
22. S.-L. Wang et al., Thermodynamically-consistent phase-field models for solidification. *Phys. Nonlinear Phenom.* **69**, 189–200 (1993).
23. I. Prigogine, *Introduction to Thermodynamics of Irreversible Processes*. Wiley, Hoboken, NJ (1967). at <http://adsabs.harvard.edu/abs/1967itti.book…..P>
24. J. Ågren, Binary and multicomponent diffusion. *Charact. Mater.* 1–16. (2002). doi:10.1002/0471266965.com014.pub2
25. L. Onsager, Theories and problems of liquid diffusion. *Ann. N. Y. Acad. Sci.* **46**, 241–265 (1945).
26. D. Sun, M. Zhu, S. Pan, and D. Raabe, Numerical modeling of dendritic growth in alloy solidification with forced convection. *Int. J. Mod. Phys. B* **23**, 1609–1614 (2009).
27. A. Younsi, A. Cartalade, and M. Lattice Boltzmann, Simulations for Anisotropic Crystal Growth of a Binary Mixture. The 15th International Heat Transfer Conference, Kyoto, Japan, August 10–15, 2014. <http://oatao.univ-toulouse.fr/11934/>
28. S. Chen and G. D. Doolen, Lattice Boltzmann method for fluid flows. *Annu. Rev. Fluid Mech.* **30**, 329–364 (1998).
29. P. Lallemand and L.-S. Luo, Theory of the lattice Boltzmann method: Dispersion, dissipation, isotropy, Galilean invariance, and stability. *Phys. Rev. E* **61**, 6546–6562 (2000).
30. Y. H. Qian, D. D'Humières, and P. Lallemand, Lattice BGK models for Navier-Stokes equation. *EPL Europhys. Lett.* **17**, 479 (1992).
31. S. M. Allen and J. W. Cahn, A microscopic theory for antiphase boundary motion and its application to antiphase domain coarsening. *Acta Metall.* **27**, 1085–1095 (1979).
32. E. W. Weisstein, "Euler-Lagrange Differential Equation," *Wolfram MathWorld*. Last updated November 6, 2017. <http://mathworld.wolfram.com/Euler-LagrangeDifferentialEquation.html>
33. J. Zhu, L.-Q. Chen, J. Shen, and V. Tikare, Coarsening kinetics from a variable-mobility Cahn-Hilliard equation: Application of a semi-implicit Fourier spectral method. *Phys. Rev. E* **60**, 3564–3572 (1999).
34. T. W. Heo and L.-Q. Chen, Phase-field modeling of nucleation in solid-state phase transformations. *JOM* **66**, 1520–1528 (2014).
35. Q. Bronchart, Y. Le Bouar, and A. Finel, New coarse-grained derivation of a phase field model for precipitation. *Phys. Rev. Lett.* **100**, 015702 (2008).
36. J. W. Cahn and J. E. Hilliard, Free energy of a nonuniform system. I. Interfacial free energy. *J. Chem. Phys.* **28**, 258 (1958).
37. N. Moelans, B. Blanpain, and P. Wollants, Quantitative analysis of grain boundary properties in a generalized phase field model for grain growth in anisotropic systems. *Phys. Rev. B* **78**, 024113 (2008).
38. B. Böttger, J. Eiken, and M. Apel, Multi-ternary extrapolation scheme for efficient coupling of thermodynamic data to a multi-phase-field model. *Comput. Mater. Sci.* **108**, Part B, 283–292 (2015).
39. N. Moelans, A quantitative and thermodynamically consistent phase-field interpolation function for multi-phase systems. *Acta Mater.* **59**, 1077–1086 (2011).
40. L.-Q. Chen and J. Shen, Applications of semi-implicit Fourier-spectral method to phase field equations. *Comput. Phys. Commun.* 147–158 (1998).doi:10.1016/S0010-4655(97)00115-X
41. A. Gilat, *Numerical Methods for Engineers and Scientists*. Wiley, Hoboken, NJ (2013).
42. P. Concus and G. H. Golub, Use of fast direct methods for the efficient numerical solution of nonseparable Elliptic equations. *SIAM J. Numer. Anal.* **10**, 1103–1120 (1973).
43. J. Shen, Efficient Spectral-Galerkin method I. Direct solvers of second- and fourth-order equations using legendre polynomials. *SIAM J. Sci. Comput.* **15**, 1489–1505 (1994).

44. J.-O. Andersson, T. Helander, L. Höglund, P. Shi, and B. Sundman, Thermo-Calc & DICTRA, computational tools for materials science. *Calphad* **26**, 273–312 (2002).
45. Pandat 8.0, Download (Free trial) – Pandat.exe. *Softw. Inf.* at <http://pandat.software.informer.com/8.0/>
46. J. Eiken, B. Böttger, and I. Steinbach, Multiphase-field approach for multicomponent alloys with extrapolation scheme for numerical application. *Phys. Rev. E* **73**, 066122 (2006).
47. K. Lejaeghere, V. Van Speybroeck, G. Van Oost, and S. Cottenier, Error estimates for solid-state density-functional theory predictions: An overview by means of the ground-state elemental crystals. *Crit. Rev. Solid State Mater. Sci.* **39**, 1–24 (2014).
48. K. Lejaeghere et al., Reproducibility in density functional theory calculations of solids. *Science* **351**, aad3000 (2016).
49. Y. Wang and J. Li, Phase field modeling of defects and deformation. *Acta Mater.* **58**, 1212–1235 (2010).
50. J. D. Waals, van der Thermodynamische theorie der capillariteit in de onderstelling van continue dichtheidsverandering (Dutch; English translation in J. Stat. Phys., 1979, 20:197). *Verhand Kon Akad V Wetensch Amst* 1, (1893).
51. T. Young, G. Peacock, and J. Leitch, *Miscellaneous works of the late Thomas Young* (London, J. Murray, 1855). at <http://archive.org/details/miscellaneouswo01youngoog>
52. R. Becker, Die Keimbildung bei der Ausscheidung in metallischen Mischkristallen. *Ann. Phys.* **424**, 128–140 (1938).
53. E. A. Guggenheim, The number of arrangements on a lattice of molecules each occupying several sites. *Trans. Faraday Soc.* **41**, 107–115 (1945).
54. R. Defay and I. Prigogine, Surface tension of regular solutions. *Trans. Faraday Soc.* **46**, 199–204 (1950).
55. Rayleigh, Lord XLIII, On Laplace's theory of capillarity. *Philos. Mag. Ser.* **5** 16, 309–315 (1883).
56. T. Murakami, S. Ono, M. Tamura, and M. Kurata, On the theory of surface tension of regular solution. *J. Phys. Soc. Jpn.* **6**, 309 (1951).
57. M. A. Hillert, Theory of nucleation of solid metallic solutions. (PhD diss., Massachusetts Institute of Technology, 1956).
58. V. L. Ginzburg and L. D. Landau, On the theory of superconductivity (1950). In *Supercond. Superfluidity* 113–137, Springer, Berlin Heidelberg, (2009). at <http://link.springer.com/chapter/10.1007/978-3-540-68008-6_4>
59. J. W. Cahn, Free energy of a nonuniform system. II. Thermodynamic basis. *J. Chem. Phys.* **30**, 1121–1124 (1959).
60. E. W. Hart, Thermodynamics of inhomogeneous systems. *Phys. Rev.* **113**, 412–416 (1959).
61. Free Boundary Problems: Theory and Applications. Eds. Pierluigi Colli, Claudio Verdi, Augusto Visintin. In International Series of Numerical Mathematics, Vol. 147. (Springer Basel AG, 2004).
62. J. B. Collins and H. Levine, Diffuse interface model of diffusion-limited crystal growth. *Phys. Rev. B* **31**, 6119–6122 (1985).
63. J. S. Langer, Models of pattern formation in first–order phase transitions, in *Dir. Condens. Matter Phys.* (1986).
64. R. Kobayashi, Modeling and numerical simulations of dendritic crystal growth. *Phys. Nonlinear Phenom.* **63**, 410–423 (1993).
65. S. G. Kim, W. T. Kim, and T. Suzuki, Phase-field model for binary alloys. *Phys. Rev. E* **60**, 7186–7197 (1999).
66. H. Löwen, J. Bechhoefer, and L. S. Tuckerman, Crystal growth at long times: critical behavior at the crossover from diffusion to kinetics-limited regimes. *Phys. Rev. A* **45**, 2399–2415 (1992).
67. A. A. Wheeler, W. J. Boettinger, and G. B. McFadden, Phase-field model for isothermal phase transitions in binary alloys. *Phys. Rev. A* **45**, 7424–7439 (1992).
68. J. Tiaden, B. Nestler, H. J. Diepers, and I. Steinbach, The multiphase-field model with an integrated concept for modelling solute diffusion. *Phys. D* **115**, 73–86 (1998).
69. W. Losert, D. A. Stillman, H. Z. Cummins, P. Kopczynski, W. J. Rappel, and A. Karma, Selection of doublet cellular patterns in directional solidification through spatially periodic perturbations. *Phys. Rev. E – Stat. Phys. Plasmas Fluids Relat. Interdiscip. Top.* **58**, 7492 (1998).
70. A. A. Wheeler, W. J. Boettinger, and G. B. McFadden, Phase-field model of solute trapping during solidification. *Phys. Rev. E* **47**, 1893–1909 (1993).
71. N. A. Ahmad, A. A. Wheeler, W. J. Boettinger, and G. B. McFadden, Solute trapping and solute drag in a phase-field model of rapid solidification. *Phys. Rev. E* **58**, 3436–3450 (1998).
72. S. G. Kim, A phase-field model with anti-trapping current for multicomponent alloys with arbitrary thermodynamic properties. *Acta Mater.* **55**, 4391–4399 (2007).
73. A. Karma, Phase-field formulation for quantitative modeling of alloy solidification. *Phys. Rev. Lett.* **87**, 115701 (2001).
74. M. Plapp, Unified derivation of phase-field models for alloy solidification from a grand-potential functional. *Phys. Rev. E* **84**, 031601 (2011).
75. H. Wang, X. Zhang, C. Lai, W. Kuang, and F. Liu, Thermodynamic principles for phase-field modeling of alloy solidification. *Curr. Opin. Chem. Eng.* **7**, 6–15 (2015).
76. M. Plapp, Phase-Field Models. In Multiphase Microfluidics: The Diffuse Interface Model. Vienna: Springer, (2012) 129–175. <http://linkinghub.elsevier.com/retrieve/pii/B9780444563699000150>
77. A. Choudhury and B. Nestler, Grand-potential formulation for multicomponent phase transformations combined with thin-interface asymptotics of the double-obstacle potential. *Phys. Rev. E* **85**, 021602 (2012).
78. B. Echebarria, R. Folch, A. Karma, and M. Plapp, Quantitative phase field model of alloy solidification. *Phys. Rev. E* **70**, (2004).
79. J. C. Ramirez, C. Beckermann, A. Karma, and H.-J. Diepers, Phase-field modeling of binary alloy solidification with coupled heat and solute diffusion. *Phys. Rev. E Stat. Nonlin. Soft Matter Phys.* **69**, 051607 (2004).
80. R. Folch and M. Plapp, Towards a quantitative phase-field model of two-phase solidification. *Phys. Rev. E* **68**, 010602 (2003).
81. R. Folch and M. Plapp, Quantitative phase-field modeling of two-phase growth. *Phys. Rev. E* **72**, 011602 (2005).
82. E. A. Brener and G. Boussinot, Kinetic cross coupling between nonconserved and conserved fields in phase field models. *Phys. Rev. E* **86**, 060601 (2012).
83. A. Gopinath, R. C. Armstrong, and R. A. Brown, Second order sharp-interface and thin-interface asymptotic

analyses and error minimization for phase-field descriptions of two-sided dilute binary alloy solidification. *J. Cryst. Growth* **291**, 272–289 (2006).
84. M. Ohno and K. Matsuura, Quantitative phase-field modeling for dilute alloy solidification involving diffusion in the solid. *Phys. Rev. E* **79**, 031603 (2009).
85. I. Steinbach, L. Zhang, and M. Plapp, Phase-field model with finite interface dissipation. *Acta Mater.* **60**, 2689–2701 (2012).
86. P. Galenko and S. Sobolev, Local nonequilibrium effect on undercooling in rapid solidification of alloys. *Phys. Rev. E* **55**, 343–352 (1997).
87. V. G. Lebedev, E. V. Abramova, D. A. Danilov, and P. K. Galenko, Phase-field modeling of solute trapping: Comparative analysis of parabolic and hyperbolic models. *Int. J. Mater. Res.* **101**, 473–479 (2010).
88. L. Zhang and I. Steinbach, Phase-field model with finite interface dissipation: Extension to multi-component multi-phase alloys. *Acta Mater.* **60**, 2702–2710 (2012).
89. H. Wang, F. Liu, G. J. Ehlen, and D. M. Herlach, Application of the maximal entropy production principle to rapid solidification: a multi-phase-field model. *Acta Mater.* **61**, 2617–2627 (2013).
90. H. Wang, W. Kuang, X. Zhang, and F. Liu, A hyperbolic phase-field model for rapid solidification of a binary alloy. *J. Mater. Sci.* **50**, 1277–1286 (2015).
91. H. Wang et al., Phase-field modeling of an abrupt disappearance of solute drag in rapid solidification. *Acta Mater.* **90**, 282–291 (2015).
92. X. Zhang, H. Wang, W. Kuang, and J. Zhang, Application of the thermodynamic extremal principle to phase-field modeling of non-equilibrium solidification in multi-component alloys. *Acta Mater.* **128**, 258–269 (2017).
93. H. Garcke, B. Nestler, and B. Stoth, On anisotropic order parameter models for multi-phase systems and their sharp interface limits. *Phys. Nonlinear Phenom.* **115**, 87–108 (1998).
94. I. Steinbach and F. Pezzolla, A generalized field method for multiphase transformations using interface fields. *Phys. Nonlinear Phenom.* **134**, 385–393 (1999).
95. A. Carré, B. Böttger, and M. Apel, Implementation of an anti-trapping current for a multicomponent multiphase-field ansatz. *J. Cryst. Growth* **380**, 5–13 (2013).
96. B. Nestler, H. Garcke, and B. Stinner, Multicomponent alloy solidification: Phase-field modeling and simulations. *Phys. Rev. E* **71**, 041609 (2005).
97. N. Moelans, B. Blanpain, and P. Wollants, Quantitative phase-field approach for simulating grain growth in anisotropic systems with arbitrary inclination and misorientation dependence. *Phys. Rev. Lett.* **101**, 025502 (2008).
98. N. Moelans, Phase-field simulations of grain growth in materials containing second-phase particles (Faseveldsimulaties van korrelgroei in materialen met tweede-fasedeeltjes). (PhD diss., KU Leuven, 2006). at <https://lirias.kuleuven.be/handle/1979/309>
99. N. Moelans, F. Wendler, and B. Nestler, Comparative study of two phase-field models for grain growth. *Comput. Mater. Sci.* **46**, 479–490 (2009).
100. J. Eiken and B. Böttger, 3D phase-field simulations of graphite growth in ductile cast iron considering interaction between local expansion and microsegregation. (2017). Last modified May 3, 2017. at <https://www.researchgate.net/publication/316650718_3D_phase-field_simulations_of_graphite_growth_in_ductile_cast_iron_considering_interaction_between_local_expansion_and_microsegregation>
101. M. Ozawa, S. Kitagawa, S. Nakayama, and Y. Takesono, Reduction of FeO in molten slags by solid Carbon in the electric arc furnace operation. *Trans. Iron Steel Inst. Jpn.* **26**, 621–628 (1986).
102. R. D. Morales, A. N. Conejo, and H. H. Rodriguez, Process dynamics of electric arc furnace during direct reduced iron melting. *Metall. Mater. Trans. B* **33**, 187–199
103. M. Barati and K. S. Coley, Kinetics of CO-CO_2 reaction with CaO-SiO_2-FeOx melts. *Metall. Mater. Trans. B* **36**, 169–178 (2005).
104. J. E. Guyer, W. J. Boettinger, J. A. Warren, and G. B. McFadden, Phase field modeling of electrochemistry. I. Equilibrium. *Phys. Rev. E Stat. Nonlin. Soft Matter Phys.* **69**, 021603 (2004).
105. J. E. Guyer, W. J. Boettinger, J. A. Warren, and G. B. McFadden, Phase field modeling of electrochemistry. II. Kinetics. *Phys. Rev. E Stat. Nonlin. Soft Matter Phys.* **69**, 021604 (2004).
106. D. Dussault and A. C. Powell, Phase field modeling of electrolysis in a slag or molten salt. In *Proc Mills Symp.* 359–371, The Institute of Materials, London (2002).
107. B. Saswata, B. Soumya, and C. Abhik, Phase-field modeling of electrochemical phenomena. *J. Indian Inst. Sci.* **96**, 257–268 (2016).
108. H. Assadi, Phase-field modelling of electro-deoxidation in molten salt. *Model. Simul. Mater. Sci. Eng.* **14**, 963 (2006).
109. W. Pongsaksawad, A. C. Powell, and D. Dussault, Phase-field modeling of transport-limited electrolysis in solid and liquid states. *J. Electrochem. Soc.* **154**, F122–F133 (2007).
110. T. H. Okabe and Y. Waseda, Producing titanium through an electronically mediated reaction. *JOM* **49**, 28–32 (1997).
111. W. Pongsaksawad, Numerical modeling of interface dynamics and transport phenomena in transport-limited electrolysis processes. (PhD diss., Massachusetts Institute of Technology, 2006). at <http://dspace.mit.edu/handle/1721.1/36209>
112. Y. Shibuta, Y. Okajima, and T. Suzuki, Phase-field modeling for electrodeposition process. *Sci. Technol. Adv. Mater.* **8**, 511–518 (2007).
113. Y. Okajima, Y. Shibuta, and T. Suzuki, A phase-field model for electrode reactions with Butler–Volmer kinetics. *Comput. Mater. Sci.* **50**, 118–124 (2010).
114. Y. Ma, X. Yao, W. Hao, L. Chen, and D. Fang, Oxidation mechanism of ZrB2/SiC ceramics based on phase-field model. *Compos. Sci. Technol.* **72**, 1196–1202 (2012).
115. L. Liang et al., Nonlinear phase-field model for electrode-electrolyte interface evolution. *Phys. Rev. E* **86**, 051609 (2012).
116. R. F. Sekerka and Z. Bi, Phase field model of multicomponent alloy slidification with hydrodynamics. In *Interfaces 21st Century New Res. Dir. Fluid Mech. Mater. Sci.* 147–166, Published By Imperial College Press And Distributed By World Scientific Publishing CO., (2002). at <http://www.worldscientific.com/doi/abs/10.1142/9781860949609_0011>

117. W. Gathright, M. Jensen, and D. Lewis, Phase field model of chemical reactions with an example of a solid electrolyte gas sensor. *Electrochem. Commun.* **13**, 520–523 (2011).
118. L. Hong, J.-M. Hu, K. Gerdes, and L.-Q. Chen, Oxygen vacancy diffusion across cathode/electrolyte interface in solid oxide fuel cells: an electrochemical phase-field model. *J. Power Sources* **287**, 396–400 (2015).
119. M. Z. Bazant, Theory of chemical kinetics and charge transfer based on nonequilibrium thermodynamics. *Acc. Chem. Res.* **46**, 1144–1160 (2013).
120. D. A. Cogswell and M. Z. Bazant, Theory of coherent nucleation in phase-separating nanoparticles. *Nano Lett.* **13**, 3036–3041 (2013).
121. T. R. Ferguson and M. Z. Bazant, Phase transformation dynamics in porous battery electrodes. *Electrochim. Acta.* **146**, 89–97 (2014). at <http://arxiv.org/abs/1401.7072>
122. T. W. Heo, L.-Q. Chen and B. C. Wood, Phase-field modeling of diffusional phase behaviors of solid surfaces: a case study of phase-separating LiXFePO4 electrode particles. *Comput. Mater. Sci.* **108**(Part B), 323–332 (2015).
123. W. Kappus and H. Horner, Surface spinodal decomposition in coherent metal-hydrogen and other alloys. *Z. Für Phys. B Condens. Matter* **27**, 215–225 (1977).
124. M. Tang and A. Karma, Surface modes of coherent spinodal decomposition. *Phys. Rev. Lett.* **108**, 265701 (2012).
125. I. Bellemans, N. Moelans, and K. Verbeken, Phase field modelling of the attachment of metallic droplets to solid particles in liquid slags: influence of interfacial energies and slag supersaturation. *Comput. Mater. Sci.* **108**(Part B), 348–357 (2015).
126. M. Asle Zaeem and H. El Kadiri, An elastic phase field model for thermal oxidation of metals: application to zirconia. *Comput. Mater. Sci.* **89**, 122–129 (2014).
127. COMSOL Multiphysics® Modeling Software. at <https://www.comsol.com/>
128. M. Apel, G. Laschet, B. Böttger, and R. Berger, Phase field modeling of microstructure formation, DSC curves, and thermal expansion for Ag-Cu brazing fillers under reactive air brazing conditions. *Adv. Eng. Mater.* **16**, 1468–1474 (2014).
129. R. Berger, M. Apel, and B. Böttger, Phase field modeling applied to reactive air brazing: Investigating reaction kinetics with focus on Oxygen exchange. *Adv. Eng. Mater.* **16**, 1475–1481 (2014).
130. about MICRESS. at <http://web.micress.de/aboutmicress.html>
131. N. Ta, L. Zhang, Y. Tang, W. Chen, and Y. Du, Effect of temperature gradient on microstructure evolution in Ni–Al–Cr bond coat/substrate systems: a phase-field study. *Surf. Coat. Technol.* **261**, 364–374 (2015). doi:10.1016/j.surfcoat.2014.10.061
132. Q. C. Sherman and P. W. Voorhees, Phase-field model of oxidation: Equilibrium. *Phys. Rev. E* **95**, 032801 (2017).
133. E. De Wilde et al., Wetting behaviour of Cu based alloys on spinel substrates in pyrometallurgical context. *Mater. Sci. Technol.* **31**, 1925–1933 (2015).
134. E. De Wilde et al., Origin and sedimentation of Cu-droplets sticking to spinel solids in pyrometallurgical slags. *Mater. Sci. Technol.* **32**, 1911–1924 (2016).
135. E. De Wilde et al., Sessile drop evaluation of high temperature copper/spinel and slag/spinel interactions. *Trans. Nonferrous Met. Soc. China* **26**, 2770–2783 (2016).
136. E. De Wilde et al., Investigation of high-temperature Slag/Copper/Spinel interactions. *Metall. Mater. Trans. B* **47**, 3421–3434 (2016).
137. E. De Wilde et al., Study of the effect of spinel composition on metallic copper losses in slags. *J. Sustain. Metall.* **3**, 416–427 (2017).
138. I. Bellemans et al., Investigation of reactive origin for attachment of Cu droplets to solid particles. *Metall. Mater. Trans. B* **48**, 2459–2468 (2017).
139. I. Bellemans, E. D. Wilde, B. Blanpain, N. Moelans, and K. Verbeken, Investigation of origin of attached Cu-Ag droplets to solid particles during high-temperature slag/copper/ppinel interactions. *Metall. Mater. Trans. B* 1–16 (2017). doi:10.1007/s11663-017-1088-4
140. L. Gránásy, T. Pusztai, D. Saylor, and J. A. Warren, Phase field theory of heterogeneous crystal nucleation. *Phys. Rev. Lett.* **98**, 035703 (2007).
141. J. A. Warren, T. Pusztai, L. Környei, and L. Gránásy, Phase field approach to heterogeneous crystal nucleation in alloys. *Phys. Rev. B* **79**, 014204 (2009).
142. L. M. Pismen and Y. Pomeau, Disjoining potential and spreading of thin liquid layers in the diffuse-interface model coupled to hydrodynamics. *Phys. Rev. E* **62**, 2480–2492 (2000).
143. A. Badillo, Quantitative phase-field modeling for wetting phenomena. *Phys. Rev. E* **91**, 033005 (2015).
144. I. Bellemans, E. De Wilde, N. Moelans, and K. Verbeken, Phase field modelling of the attachment of metallic droplets to solid particles in liquid slags: influence of particle characteristics. *Acta Mater.* **101**, 172–180 (2015).
145. I. Bellemans, N. Moelans, and K. Verbeken, Influence of rigid body motion on the wetting and attachment of metallic droplets to solid particles in liquid slags—a phase field study. *Miner. Metall. Process.* (Submitted).
146. W. Villanueva, K. Grönhagen, G. Amberg, and J. Ågren, Multicomponent and multiphase modeling and simulation of reactive wetting. *Phys. Rev. E* **77**, 056313 (2008).
147. W. Villanueva, W. J. Boettinger, J. A. Warren, and G. Amberg, Effect of phase change and solute diffusion on spreading on a dissolving substrate. *Acta Mater.* **57**, 6022–6036 (2009).
148. W. Villanueva, W. J. Boettinger, G. B. McFadden, and J. A. Warren, A diffuse-interface model of reactive wetting with intermetallic formation. *Acta Mater.* **60**, 3799–3814 (2012).
149. D. Wheeler, J. A. Warren, and W. J. Boettinger, Modeling the early stages of reactive wetting. *Phys. Rev. E* **82**, 051601 (2010).
150. F. Wang and B. Nestler, A phase-field study on the formation of the intermetallic Al_2Au phase in the Al–Au system. *Acta Mater.* **95**, 65–73 (2015).
151. A. D. Pelton, S. A. Degterov, G. Eriksson, C. Robelin, and Y. Dessureault, The modified quasichemical model I—Binary solutions. *Metall. Mater. Trans. B* **31**, 651–659 (2000).
152. A. D. Pelton and P. Chartrand, The modified quasi-chemical model: Part II. Multicomponent solutions. *Metall. Mater. Trans. A* **32**, 1355–1360 (2001).
153. P. Chartrand and A. D. Pelton, The modified quasi-chemical model: Part III. Two sublattices. *Metall. Mater. Trans. A* **32**, 1397–1407 (2001).
154. A. D. Pelton, P. Chartrand, and G. Eriksson, The modified quasi-chemical model: Part IV. Two-sublattice

quadruplet approximation. *Metall. Mater. Trans. A* **32**, 1409–1416 (2001).
155. J. Heulens, B. Blanpain, and N. Moelans, A phase field model for isothermal crystallization of oxide melts. *Acta Mater.* **59**, 2156–2165 (2011).
156. J. Heulens, B. Blanpain, and N. Moelans, Phase field modeling of the crystallization of $FeOx–SiO_2$ melts in contact with an oxygen-containing atmosphere. *Chem. Geol.* **290**, 156–162 (2011).
157. J.-J. Liu, J. Heulens, M.-X. Guo and N. Moelans, Isothermal crystal growth behavior of $CaSiO_3$ in ternary oxide melts. *J. Inorg. Mater.* **31**, 547 (2016).
158. J.-J. Liu et al., In-situ observation of isothermal $CaSiO_3$ crystallization in $CaO–Al_2O_3–SiO_2$ melts: a study of the effects of temperature and composition. *J. Cryst. Growth* **402**, 1–8 (2014).
159. J. Heulens, B. Blanpain, and N. Moelans, Analysis of the isothermal crystallization of $CaSiO_3$ in a $CaO–Al_2O_3–SiO_2$ melt through in situ observations. *J. Eur. Ceram. Soc.* **31**, 1873–1879 (2011).
160. J. Liu, J. Zou, M. Guo, and N. Moelans, Phase field simulation study of the dissolution behavior of Al_2O_3 into $CaO–Al_2O_3–SiO_2$ slags. *Comput. Mater. Sci.* **119**, 9–18 (2016).
161. J. Liu, F. Verhaeghe, M. Guo, B. Blanpain, and P. Wollants, In situ observation of the dissolution of spherical alumina particles in $CaO–Al_2O_3–SiO_2$ melts. *J. Am. Ceram. Soc.* **90**, 3818–3824 (2007).